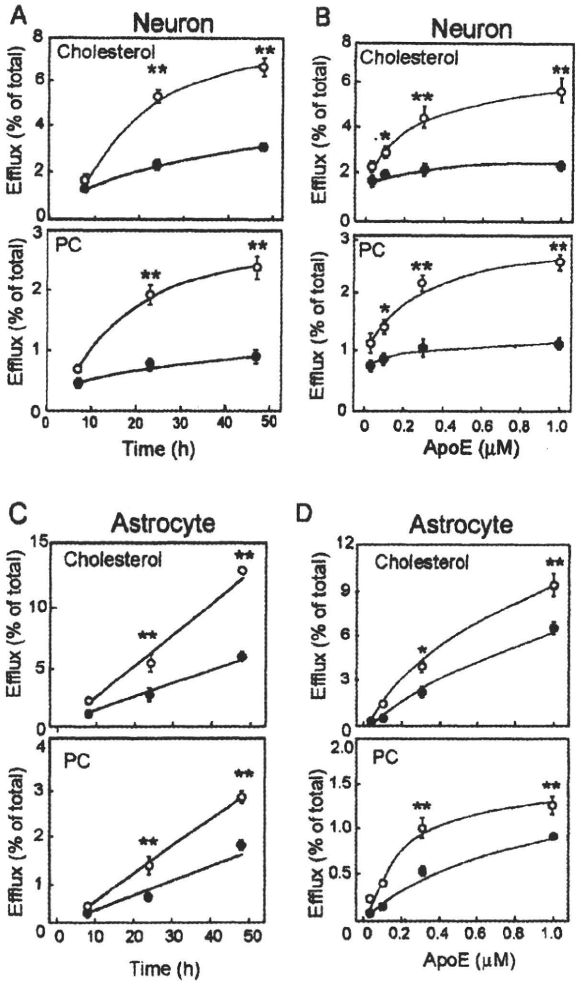

Fig. 2. Time- and dose-dependent lipid efflux mediated by 22-kDa-ApoE fragment. Cultured neurons and astrocytes were prepared, maintained, and labeled with [^{14}C]acetate as described in the legend for Fig. 1. For determination of the time-dependent lipid release from neurons (**A**) and astrocytes (**C**), each culture was exposed to 22-kDa-ApoE3 (open circle) and 22-kDa-ApoE4 (closed circle) at 0.3 μM for 8, 24, and 48 hr. For determination of the dose-dependent lipid release from neurons (**B**) and astrocytes (**D**), each culture was exposed to 22-kDa-ApoE3 (open circle) and 22-kDa-ApoE4 (closed circle) at varying concentrations for 24 hr. The lipids released into the media and the lipids retained in the cells were determined as described in Experimental Procedures. (**B**) For determination of Data are means ± SE of four samples. $*P < 0.05$ and $**P < 0.0005$ vs. 22-kDa-ApoE4 at each time point. The basal value of cholesterol and PC efflux in the absence of ApoEs are less than 0.8 ± 0.05 and 0.66 ± 0.11, respectively (**A**), and 0.59 ± 0.04 and 0.39 ± 0.04, respectively (**B**).

boxyl- terminal region longer than 250 amino acid residues lost the additional effect of the carboxyl-terminal region on lipid efflux. The levels of cholesterol and PC efflux induced by mt-ApoE4 recovered significantly but partially, and they did not reach those induced by intact ApoE3, similar to the result shown in Figure 1. Similar results were observed when ApoE-deficient astrocyte cultures were used (Fig. 3B).

The above results suggest that the amino-terminal domain basically determines the ability of ApoE to induce lipid efflux and that the carboxyl-terminal region enhances this ability when the amino and carboxyl domain interaction is absent. Because the absence or presence of cysteine at position 112 in the amino-terminal domain differentiates ApoE3 from ApoE4, it is possible to assume that this one-amino-acid difference results in intra- or intermolecular structural differences leading to the domain interaction or dimerization, respectively. Thus, we examined the effect of the dimer formation of 22-kDa-ApoE3 through disulfide bonds on lipid efflux from neurons and cultured astrocytes. To determine directly whether the dimeric form of 22-kDa-ApoE3 induces greater lipid efflux from astrocytes than the monomeric form, the pure dimeric form of 22-kDa-ApoE3 was prepared as described in Experimental Procedures. To obtain a solution containing the pure monomeric form of 22-kDa-ApoE3, 22-kDa-ApoE3 was dissolved in 5 M guanidine–HCl and 10 mM DTT. The resulting solutions were dialyzed against PBS at 4°C for 16 hr and used for the experiment. The purity of dimer and monomer in each sample was confirmed by Western blot analysis (Fig. 4). We also used 22-kDa-ApoE4 as monomeric ApoE molecule for the experiment that used astrocyte cultures because 22-kDa-ApoE4 contains no cysteine and it remains monomeric (Fig. 4B). The results demonstrated that dimeric form of 22-kDa-ApoE3 induced greater lipid efflux than the monomeric form of 22-kDa-ApoE3 and 22-kDa-ApoE4 in both neuron and astrocyte cultures (Fig. 4). Importantly, regardless of ApoE isoform, monomeric 22-kDa-ApoEs induces similar level of lipid efflux (Fig. 4B).

To determine whether such is the case for intact ApoEs, we examined the effect of the dimer formation of ApoE3 through disulfide bonds on lipid efflux from cultured neurons. We obtained dimer-enriched ApoE3 solutions by using a SulfoLink kit as described under Experimental Procedures. We also used ApoE3 solutions prepared without dimer enrichment, containing monomers and relatively few dimers. We also examined the effect of monomeric ApoEs, namely ApoE4 and ApoE3, whose cysteine was modified by carboxamidomethylation (ApoE3-CM). The levels of cholesterol and PC released from neurons treated with dimer-enriched ApoE3 were 2.9- and 7.6-fold greater than those released from neurons treated with ApoE3 and ApoE3 monomers (ApoE3-CM), respectively (Fig. 5). The effects of ApoE3-CM and ApoE4 on lipid efflux were similar. A Western blot analysis of each sample was performed and results show that the samples contained different amounts of dimers (Fig. 5B). The percentages of ApoE3 dimers as calculated by a densitometric analysis of the bands on the Western blot films were 64.5%,

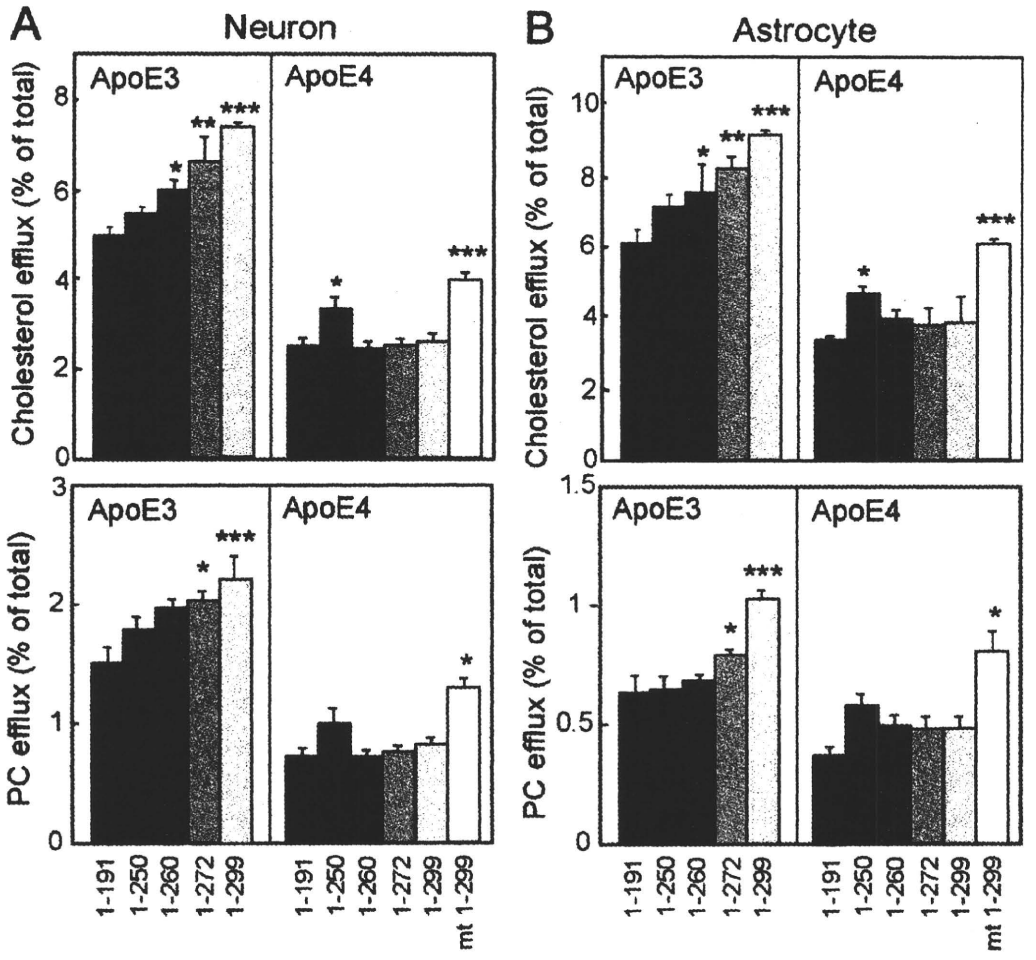

Fig. 3. Cooperative effects of amino- and carboxyl-terminal regions of ApoE on lipid efflux. Neurons and astrocytes were prepared, maintained, and labeled with [^{14}C]acetate as described in the legend for Fig. 1. The neurons (**A**) and astrocytes (**B**) were then exposed to ApoE with carboxyl-terminal regions of various lengths including 1–250, 1–260, 1–272, and 1–299 (full-length ApoE) at 0.3 μM for 24 hr, and the lipids released into the media and the lipids retained in the cells were determined as described in Experimental Procedures. For comparison, the effect of mt-ApoE4 was also determined. Data are means ± SE of four samples. $*P < 0.05$, $**P < 0.005$, and $***P < 0.0001$ vs. 22-kDa-ApoE (1–191). The basal value of cholesterol and PC efflux in the absence of ApoEs are less than 0.8 ± 0.05 and 0.66 ± 0.11, respectively (A, B).

36.9%, 1.8%, and 1.4% in the dimer-enriched ApoE3, non-dimer-enriched ApoE3, ApoE3-CM, and ApoE4 samples, respectively.

Next we determined the involvement of ABCA1 in 22-kDa-ApoEs-induced lipid efflux. The neuron cultures were treated with 22-kDa-ApoE3 dimers, 22-kDa-ApoE3 monomers, or 22-kDa-ApoE4 (monomers) concomitant with 10 μM of 22-hydroxycholesterol, an LXR ligand to up-regulate *ABCA1* gene expression (Wang et al., 2001), and the cultures were maintained for 24 hr. After 24 hr incubation, the level of lipids released into the medium was determined. The ABCA1 expression level was enhanced when the neurons were treated with 22-hydroxycholesterol (Fig. 6A). The levels of lipids released by these ApoE fragments were significantly enhanced when the cultures were concomitantly treated with 22-hydroxycholesterol (Fig. 6B). These results suggest that ABCA1 plays a key role in 22-kDa-ApoEs-mediated lipid efflux in neurons. In support of this notion, we have observed that the treatment of neurons with glyburide, an inhibitor of the ABCA1 transporter, resulted in decreased levels of 22-kDa-ApoE3-mediated cholesterol efflux (Fig. 6C). We further examined the effect of ABCA1 knockdown on 22-kDa ApoEs-mediated lipid efflux by using specific siRNAs. The knockdown of ABCA1 in neurons significantly reduced lipid efflux induced by 22-kDa-ApoE3 dimers (Fig. 7).

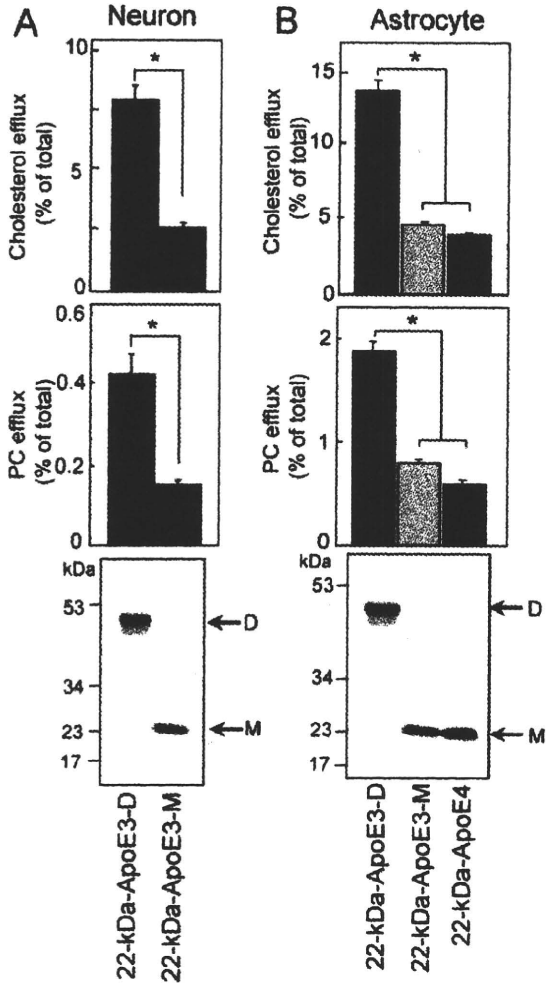

Fig. 4. The ability of 22-kDa-ApoE to induce lipid efflux depends on the ApoE self-association state, i. e., monomer vs dimer. Preparation of 22-kDa-ApoE3 dimer (22-kDa-ApoE3-D), monomer (22-kDa-ApoE3-M), or 22-kDa-ApoE4 monomer was performed as described in Experimental Procedures. **A:** The same amount of 22-kDa-ApoE3-D or 22-kDa-ApoE3-M was subjected to SDS-PAGE under nonreducing conditions, and Western blot analysis was performed with the anti-ApoE antibody AB947. D; dimers, M; monomer. Neuron cultures were prepared, maintained, and labeled with [^{14}C]acetate and exposed to 22-kDa-ApoE3-D or 22-kDa-ApoE3-M at 0.3 μM for 24 hr. The cholesterol and PC efflux by dimeric and monomeric 22-kDa-ApoE3 was determined. **B:** The same amount of 22-kDa-ApoE3 dimers, 22-kDa-ApoE3 monomers, and 22-kDa-ApoE4 monomers was subjected to SDS-PAGE under nonreducing conditions, and Western blot analysis was performed with the anti-ApoE antibody AB947. D; dimers, M; monomer. Astrocyte cultures were prepared, maintained, and labeled with [^{14}C]acetate and exposed to 22-kDa-ApoE3-D, 22-kDa-ApoE3-M, or 22-kDa-ApoE4 monomer at 0.3 μM for 24 hr. The cholesterol and PC efflux by dimeric and monomeric 22-kDa-ApoE3, and monomeric 22-kDa-ApoE4 was determined. Data are means ± SE of four samples. $*P < 0.0001$ vs. 22-kDa-ApoE3. The basal value of cholesterol and PC efflux in the absence of ApoEs are less than 1.41 ± 0.06 and 0.55 ± 0.03, respectively (A, B).

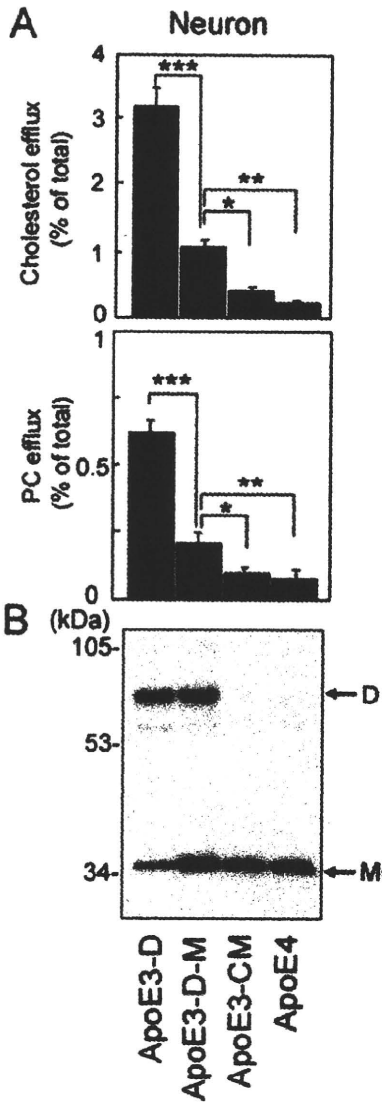

Fig. 5. Effect of intact ApoE dimers on lipid efflux from cultured neurons. A dimer-rich ApoE3 solution was obtained with a column that traps SH residues (monomeric ApoE3s). Carboxamidomethylated ApoE with iodoacetamide was prepared as described in Experimental Procedures. Neuronal cultures were prepared, maintained, and labeled with [^{14}C]acetate and exposed to dimer-enriched ApoE3, ApoE3, ApoE3-CM, and ApoE4 at 0.3 μM for 24 hr. **A:** The levels of cholesterol and PC released into the media and those retained in the cells were determined as described in Experimental Procedures. **B:** To determine the amount of dimers in the samples, Western blot analysis was performed under nonreducing conditions with anti-ApoE antibody AB947 used as the primary antibody. Data are means ± SE of four samples. $*P < 0.01$, $**P < 0.001$, $***P < 0.0001$. The basal value of cholesterol and PC efflux in the absence of ApoEs are 1.54 ± 0.05 and 0.56 ± 0.05, respectively.

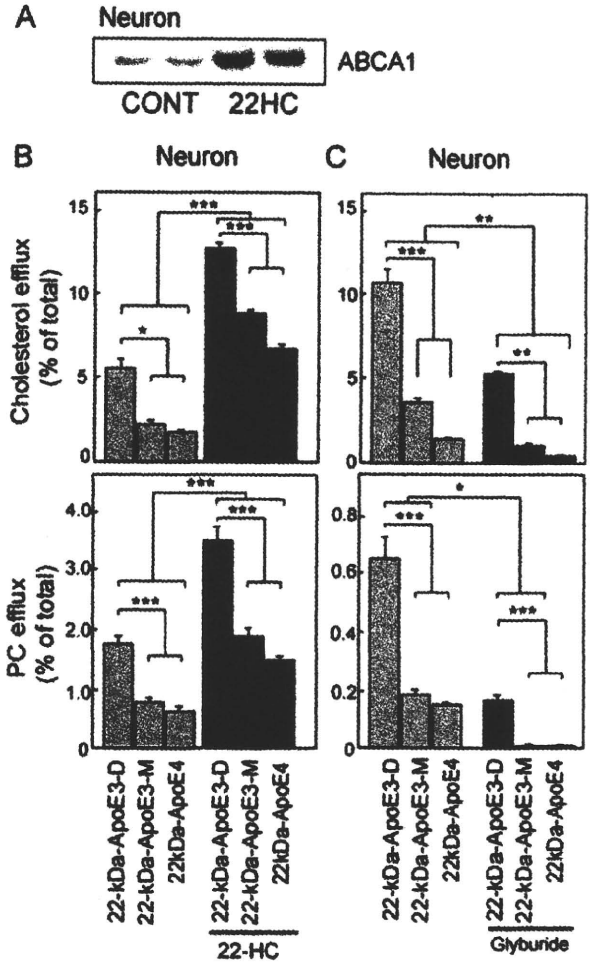

Fig. 6. The effect of 22-hydroxycholesterol and glyburide on 22-kDa-ApoEs-induced lipid efflux. Neuron cultures were prepared, maintained, and labeled with [^{14}C]acetate as described in Fig. 1, and exposed to 22-kDa-ApoE3 dimer (22-kDa-ApoE3-D), 22-kDa-ApoE3 monomer (22-kDa-ApoE3-M), or 22-kDa-ApoE4 at a concentration of 0.3 μM in the presence of 22-hydroxycholesterol (HC) at a concentration of 10 μM for 24 hr. (**A**) The expression level of ABCA1 in the cultures for each treatment was determined by Western blot analysis, and (**B**) the lipids released into the media and the lipids retained in the cells were determined. (**C**) [^{14}C]acetate-labeled neuron cultures were exposed to 22-kDa-ApoE3 dimer (22-kDa-ApoE3-D), 22-kDa-ApoE3 monomer (22-kDa-ApoE3-M), or 22-kDa-ApoE4 at a concentration of 0.3 μM in the presence of glyburide (500 μM) for 24 hr. The lipids released into the media and the lipids retained in the cells were determined. Data are means ± SE of four samples. $*P < 0.05$, $**P < 0.01$, and $***P < 0.0005$. Three independent experiments showed similar results. The basal value of cholesterol and PC efflux in the absence of ApoEs are 5.45 ± 0.51 and 0.58 ± 0.06, respectively.

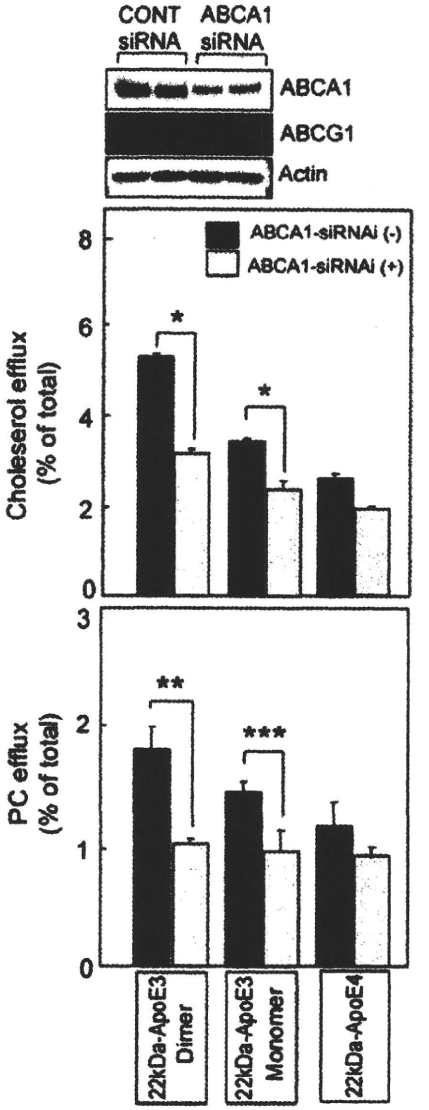

Fig. 7. Lipid efflux by 22-kDa-ApoEs is mediated by ABCA1. The primary neurons, which had been labeled with [^{14}C]acetate and treated with siRNA against ABCA1 for 48 hr, were exposed to 22-kDa-ApoE3 dimer (22-kDa-ApoE3-D) or 22-kDa-ApoE3 monomer (22-kDa-ApoE3-M) at a concentration of 0.3 μM, and maintained for 24 hr. The lipids released into the media and the lipids retained in the cells were then determined as described in Experimental Procedures. Data are means ± SE of four samples. $*P < 0.0001$, $**P < 0.002$, $***P < 0.02$. Three independent experiments showed similar results. The basal value of cholesterol and PC efflux in the absence of ApoEs are 0.89 ± 0.08 and 0.97 ± 0.14, respectively. Those values are 0.84 ± 0.08 and 0.46 ± 0.07 in the siABCA1 experiment.

DISCUSSION

We showed here that lipid efflux induced by ApoE is mainly mediated by the amino-terminal domain of ApoE and modified by the carboxyl-terminal domain. What we found are that the amino-terminal domain of ApoE induces lipid efflux in an isoform-dependent manner and the carboxyl-terminal domain enhances lipid efflux mediated by the amino-terminal domain of ApoE3. In contrast, the carboxyl-terminal domain does not strengthen the lipid efflux mediated by the amino-terminal domain of ApoE4 because of the domain interaction between the amino- and carboxyl-terminal domains. We also found that the lipid efflux induced by these ApoEs is mediated in an ABCA1-dependent manner.

Two of the main findings in this study are that the amino-terminal domain of ApoE, 22-kDa-ApoE, induces lipid efflux and that the extent of lipids released by the amino-terminal domain of ApoE, 22-kDa-ApoE3, is approximately 66% of that induced by intact ApoE3. The carboxyl-terminal domain synergistically and additively modifies lipid efflux mediated by 22-kDa-ApoE3. The additional contribution of the carboxyl-terminal domain is not observed in the case of ApoE4. Basically, 22-kDa-ApoE4 has a very weak ability to induce lipid efflux; moreover, the carboxyl-terminal region of ApoE does not effectively or additively enhance the lipid efflux mediated by 22-kDa-ApoE4. The lack of an additive effect by the carboxyl-terminal region on lipid efflux is likely due to the domain interaction, because an ApoE4 fragment ending at 250 (ApoE1–250) significantly gains in ability to release lipids; however, a carboxyl-terminal region longer than the amino acid 255, glutamate, which interacts with arginine at 61 (called the domain interaction; Dong and Weisgraber, 1996), does not induce any additive effect on lipid efflux induced by 22-kDa-ApoE4.

Another important finding regarding the effect of the domain interaction is that lipid efflux induced by mt-ApoE4 shows only a partial recovery toward the level exhibited by ApoE3. This indicates that the presence or absence of the amino and carboxyl domain interaction cannot completely explain ApoE-isoform-dependent lipid efflux mediated by intact ApoE and that other mechanisms are responsible for such ApoE-isoform dependency. This is supported by the finding of this study that 22-kDa-ApoE, which has no carboxyl-terminal region and thus has no domain interaction, induces lipid release in an ApoE-isoform-dependent manner.

We have already shown that α-helix formation is required for the high-affinity binding of apolipoprotein A-I to lipids (Saito et al., 2004), and that the binding capacity of 22-kDa-ApoE3 is lower than that of 22-kDa-ApoE4 for lipid particles (Saito et al., 2003). On the basis of the facts that the structural stabilities of 22-kDa-ApoE3 and 22-kDa-ApoE4 determine their binding affinity to lipids (Morrow et al., 2002; Segall et al., 2002; Weers et al., 2003) and that 22-kDa-ApoE4 is less stable than 22-kDa-ApoE3 (Morrow et al., 2000), it is reasonable to predict that the level of lipid efflux induced by 22-kDa-ApoE4 would be greater than that induced by 22-kDa-ApoE3. However, our results show the opposite, indicating that ApoE-isoform-dependent cholesterol efflux is unlikely to be explained by a simple theory linking the structural difference between these two fragments with their binding affinity to lipids.

Therefore, the question arises as to what is the mechanism underlying the isoform dependency of 22-kDa-ApoE-induced lipid efflux. It is possible to assume that 22-kDa-ApoE induces lipid efflux, because the 22-kDa domain contains an amphipathic four-helix bundle (Wilson et al., 1991), and it can bind to and reorganize phospholipid vesicles to form discoidal complexes (Lu et al., 2000; Segall et al., 2002). Surprisingly, 22-kDa-ApoE-induced lipid efflux is ApoE-isoform dependent. Such isoform dependency is likely to be caused by the presence or absence of cysteine at residue 112, which may result in intra- or intermolecular structural changes, forming dimers of 22-kDa-ApoE through disulfide bonds. More direct evidence that the dimeric form of 22-kDa-ApoE3 induces greater lipid efflux from cultured neurons and astrocytes than the monomeric form (Fig. 4) supports this idea. Previous reports have demonstrated that cellular cholesterol efflux is induced by many apolipoproteins in their lipid-free form, including ApoA-I, ApoA-II, ApoA-IV, and ApoCIII in addition to ApoE, all of which harbor multiple segments of amphiphilic helices (Segrest et al., 1992); the reaction still occurs with shorter apolipoproteins but to a lesser extent and only at high concentrations (Bielicki et al., 1992). Synthetic amphipathic helical peptides that mimic the physical properties of amphipathic helical segments of apolipoproteins can also induce cholesterol efflux as long as the peptide has at least two such helical segments (Mendez et al., 1994; Yancey et al., 1995). Consistent with these lines of evidence, when human ApoA-II, a disulfide-linked dimer, is reduced to a carboxyamidomethylation monomeric form, the ability of ApoA-II to induce cholesterol efflux is significantly decreased (Hara et al., 1992). In addition, the disulfide- linked homodimer of ApoE3 has been identified not only in cell culture medium (Gong et al., 2002), but also in human plasma (Weisgraber and Shinto, 1991). The mechanism by which the ApoE and ApoA-II dimers gain their functions to release higher amounts of lipids than ApoE and ApoA-II monomers, respectively, remains to be elucidated.

ABCA1 is involved in apolipoprotein-induced lipid efflux, including that mediated by ApoA-I (Brooks-Wilson et al., 1999; Lawn et al., 1999) and ApoE (Remaley et al., 2001; Krimbou et al., 2004). Regarding its effect on lipid efflux, the carboxyl-terminal fragment of ApoE (10-kDa-ApoE) induces a strong lipid efflux from non-CNS cells such as macrophages and ABCA1 plays a critical role in this efflux (Vedhachalam et al., 2007). Interestingly, contrary to these findings, 10-kDa-ApoE does not induce lipid efflux from the cultured neurons and astrocytes (Fig. 1). The reason for this discrepancy

remains unknown; however, the cell type difference may be a likely reason. In support of this notion, even intact ApoE3 induces a very low level of lipid efflux from macrophages or fibroblasts, and ABCA1 transfection induces a marked lipid efflux mediated by intact ApoE3 in these cells (Smith et al., 1996; Remaley et al., 2001). In contrast, intact ApoE3 itself induces marked lipid efflux from astrocytes without ABCA1 transfection as shown in this study. This may be because apolipoprotein-mediated cholesterol efflux is only apparent in growth-arrested cells (Mendez, 1997).

We have observed that pretreatment with 22-hydroxylcholesterol enhanced ABCA1 expression in neurons and cholesterol efflux induced by ApoE, suggesting that ABCA1 is involved in ApoE- and 22-kDa-ApoE3-mediated cholesterol efflux (Fig. 6). The involvement of ABCA1 has been also demonstrated by the fact that the knockdown of ABCA1 significantly reduced lipid efflux induced by 22-kDa ApoEs (Fig. 7). One cannot exclude the possibility that factors other than ABCA1 that are relevant to biological mechanisms are involved because the involvement of ATP-binding cassette protein G1 has been reported previously (Karten et al., 2006; Kim et al., 2007); however, the lines of evidence in our present study suggest that lipid efflux from cultured neurons induced by ApoE or an ApoE fragment is mediated by ABCA1 function.

It is reasonable to assume that the disruption of the ApoE4 domain interaction by, for example, small molecules that create the ApoE3-like structure is a potential therapeutic target in neurodegenerative diseases including AD (Mahley et al., 2006). However, if the role of ApoE in HDL generation and its supply to neurons are critically involved in neurodegeneration in AD, other approaches that do not modulate the acceptor function, but modulate the cellular factors including ABCA1 expression and subsequent HDL generation, could also be candidate therapeutic targets.

REFERENCES

Bielicki JK, Johnson WJ, Weinberg RB, Glick JM, Rothblat GH. 1992. Efflux of lipid from fibroblasts to apolipoproteins: dependence on elevated levels of cellular unesterified cholesterol. J Lipid Res 33:1699–1709.

Borghini I, Barja F, Pometta D, James RW. 1995. Characterization of subpopulations of lipoprotein particles isolated from human cerebrospinal fluid. Biochim Biophys Acta 1255:192–200.

Boyles JK, Pitas RE, Wilson E, Mahley RW, Taylor JM. 1985. Apolipoprotein E associated with astrocytic glia of the central nervous system and with nonmyelinating glia of the peripheral nervous system. J Clin Invest 76:1501–1513.

Brooks-Wilson A, Marcil M, Clee SM, Zhang LH, Roomp K, van Dam M, Yu L, Brewer C, Collins JA, Molhuizen HO, Loubser O, Ouelette BF, Fichter K, Ashbourne-Excoffon KJ, Sensen CW, Scherer S, Mott S, Denis M, Martindale D, Frohlich J, Morgan K, Koop B, Pimstone S, Kastelein JJ, Hayden MR. 1999. Mutations in ABC1 in Tangier disease and familial high-density lipoprotein deficiency. Nat Genet 22: 336–345.

Corder EH, Saunders AM, Strittmatter WJ, Schmechel DE, Gaskell PC, Small GW, Roses AD, Haines JL, Pericak-Vance MA. 1993. Gene dose of apolipoprotein E type 4 allele and the risk of Alzheimer's disease in late onset families [see comments]. Science 261:921–923.

Demeester N, Castro G, Desrumaux C, De Geitere C, Fruchart JC, Santens P, Mulleners E, Engelborghs S, De Deyn PP, Vandekerckhove J, Rosseneu M, Labeur C. 2000. Characterization and functional studies of lipoproteins, lipid transfer proteins, and lecithin:cholesterol acyltransferase in CSF of normal individuals and patients with Alzheimer's disease. J Lipid Res 41:963–974.

Dong LM, Weisgraber KH. 1996. Human apolipoprotein E4 domain interaction. Arginine 61 and glutamic acid 255 interact to direct the preference for very low density lipoproteins. J Biol Chem 271:19053–19057.

Franceschini G, Calabresi L, Tosi C, Gianfranceschi G, Sirtori CR, Nichols AV. 1990. Apolipoprotein AIMilano. Disulfide-linked dimers increase high density lipoprotein stability and hinder particle interconversion in carrier plasma. J Biol Chem 265:12224–12231.

Gong JS, Kobayashi M, Hayashi H, Zou K, Sawamura N, Fujita SC, Yanagisawa K, Michikawa M. 2002. Apolipoprotein E (ApoE) isoform-dependent lipid release from astrocytes prepared from human ApoE3 and ApoE4 knock-in mice. J Biol Chem 277:29919–29926.

Hara H, Komaba A, Yokoyama S. 1992. Alpha-helical requirements for free apolipoproteins to generate HDL and to induce cellular lipid efflux. Lipids 27:302–304.

Hatters DM, Budamagunta MS, Voss JC, Weisgraber KH. 2005. Modulation of apolipoprotein E structure by domain interaction: differences in lipid-bound and lipid-free forms. J Biol Chem 280:34288–34295.

Karten B, Campenot RB, Vance DE, Vance JE. 2006. Expression of ABCG1, but not ABCA1, correlates with cholesterol release by cerebellar astroglia. J Biol Chem 281:4049–4057.

Kim WS, Rahmanto AS, Kamili A, Rye KA, Guillemin GJ, Gelissen IC, Jessup W, Hill AF, Garner B. 2007. Role of ABCG1 and ABCA1 in regulation of neuronal cholesterol efflux to apolipoprotein E discs and suppression of amyloid-beta peptide generation. J Biol Chem 282:2851–2861.

Krimbou L, Denis M, Haidar B, Carrier M, Marcil M, Genest J Jr. 2004. Molecular interactions between apolipoprotein E and the ATP-binding cassette transporter A1 (ABCA1): impact on ApoE lipidation. J Lipid Res 46:1457–1465.

LaDu MJ, Gilligan SM, Lukens JR, Cabana VG, Reardon CA, Van Eldik LJ, Holtzman DM. 1998. Nascent astrocyte particles differ from lipoproteins in CSF. J Neurochem 70:2070–2081.

Lawn RM, Wade DP, Garvin MR, Wang X, Schwartz K, Porter JG, Seilhamer JJ, Vaughan AM, Oram JF. 1999. The Tangier disease gene product ABC1 controls the cellular apolipoprotein-mediated lipid removal pathway. J Clin Invest 104:R25–31.

Lu B, Morrow JA, Weisgraber KH. 2000. Conformational reorganization of the four-helix bundle of human apolipoprotein E in binding to phospholipid. J Biol Chem 275:20775–20781.

Mahley RW, Weisgraber KH, Huang Y. 2006. Apolipoprotein E4: a causative factor and therapeutic target in neuropathology, including Alzheimer's disease. Proc Natl Acad Sci U S A 103:5644–5651.

Mendez AJ. 1997. Cholesterol efflux mediated by apolipoproteins is an active cellular process distinct from efflux mediated by passive diffusion. J Lipid Res 38:1807–1821.

Mendez AJ, Anantharamaiah GM, Segrest JP, Oram JF. 1994. Synthetic amphipathic helical peptides that mimic apolipoprotein A-I in clearing cellular cholesterol. J Clin Invest 94:1698–1705.

Michikawa M, Fan QW, Isobe I, Yanagisawa K. 2000. Apolipoprotein E exhibits isoform-specific promotion of lipid efflux from astrocytes and neurons in culture. J Neurochem 74:1008–1016.

Michikawa M, Gong JS, Fan QW, Sawamura N, Yanagisawa K. 2001. A novel action of Alzheimer's amyloid b-protein (Ab): oligomeric Ab promotes lipid release. J Neurosci 21:7226–7235.

Molander-Melin M, Blennow K, Bogdanovic N, Dellheden B, Mansson JE, Fredman P. 2005. Structural membrane alterations in Alzheimer brains found to be associated with regional disease development; increased density of gangliosides GM1 and GM2 and loss of cholesterol in detergent-resistant membrane domains. J Neurochem 92:171–182.

Morrow JA, Segall ML, Lund-Katz S, Phillips MC, Knapp M, Rupp B, Weisgraber KH. 2000. Differences in stability among the human apolipoprotein E isoforms determined by the amino-terminal domain. Biochemistry 39:11657–11666.

Morrow JA, Hatters DM, Lu B, Hochtl P, Oberg KA, Rupp B, Weisgraber KH. 2002. Apolipoprotein E4 forms a molten globule. A potential basis for its association with disease. J Biol Chem 277:50380–50385.

Nakai M, Kawamata T, Taniguchi T, Maeda K, Tanaka C. 1996. Expression of apolipoprotein E mRNA in rat microglia. Neurosci Lett 211:41–44.

Pitas RE, Boyles JK, Lee SH, Foss D, Mahley RW. 1987a. Astrocytes synthesize apolipoprotein E and metabolize apolipoprotein E–containing lipoproteins. Biochim Biophys Acta 917:148–161.

Pitas RE, Boyles JK, Lee SH, Hui D, Weisgraber KH. 1987b. Lipoproteins and their receptors in the central nervous system. Characterization of the lipoproteins in cerebrospinal fluid and identification of apolipoprotein B,E(LDL) receptors in the brain. J Biol Chem 262:14352–14360.

Raffai RL, Dong LM, Farese RV Jr, Weisgraber KH. 2001. Introduction of human apolipoprotein E4 "domain interaction" into mouse apolipoprotein E. Proc Natl Acad Sci U S A 98:11587–11591.

Ramaswamy G, Xu Q, Huang Y, Weisgraber KH. 2005. Effect of domain interaction on apolipoprotein E levels in mouse brain. J Neurosci 25:10658–10663.

Remaley AT, Stonik JA, Demosky SJ, Neufeld EB, Bocharov AV, Vishnyakova TG, Eggerman TL, Patterson AP, Duverger NJ, Santamarina-Fojo S, Brewer HB Jr. 2001. Apolipoprotein specificity for lipid efflux by the human ABCAI transporter. Biochem Biophys Res Commun 280:818–823.

Roheim PS, Carey M, Forte T, Vega GL. 1979. Apolipoproteins in human cerebrospinal fluid. Proc Natl Acad Sci U S A 76:4646–4649.

Saito H, Dhanasekaran P, Baldwin F, Weisgraber KH, Lund-Katz S, Phillips MC. 2001. Lipid binding-induced conformational change in human apolipoprotein E. Evidence for two lipid-bound states on spherical particles. J Biol Chem 276:40949–40954.

Saito H, Dhanasekaran P, Baldwin F, Weisgraber KH, Phillips MC, Lund-Katz S. 2003. Effects of polymorphism on the lipid interaction of human apolipoprotein E. J Biol Chem 278:40723–40729.

Saito H, Dhanasekaran P, Nguyen D, Deridder E, Holvoet P, Lund-Katz S, Phillips MC. 2004. Alpha-helix formation is required for high affinity binding of human apolipoprotein A-I to lipids. J Biol Chem 279:20974–20981.

Segall ML, Dhanasekaran P, Baldwin F, Anantharamaiah GM, Weisgraber KH, Phillips MC, Lund-Katz S. 2002. Influence of apoE domain structure and polymorphism on the kinetics of phospholipid vesicle solubilization. J Lipid Res 43:1688–1700.

Segrest JP, Jones MK, De Loof H, Brouillette CG, Venkatachalapathi YV, Anantharamaiah GM. 1992. The amphipathic helix in the exchangeable apolipoproteins: a review of secondary structure and function. J Lipid Res 33:141–166.

Smith JD, Miyata M, Ginsberg M, Grigaux C, Shmookler E, Plump AS. 1996. Cyclic AMP induces apolipoprotein E binding activity and promotes cholesterol efflux from a macrophage cell line to apolipoprotein acceptors. J Biol Chem 271:30647–30655.

Strittmatter WJ, Saunders AM, Schmechel D, Pericak-Vance M, Enghild J, Salvesen GS, Roses AD. 1993. Apolipoprotein E: high-avidity binding to beta-amyloid and increased frequency of type 4 allele in late-onset familial Alzheimer disease. Proc Natl Acad Sci U S A 90:1977–1981.

Vedhachalam C, Narayanaswami V, Neto N, Forte TM, Phillips MC, Lund-Katz S, Bielicki JK. 2007. The C-terminal lipid-binding domain of apolipoprotein E is a highly efficient mediator of ABCA1-dependent cholesterol efflux that promotes the assembly of high-density lipoproteins. Biochemistry 46:2583–2593.

Wang N, Silver DL, Thiele C, Tall AR. 2001. ATP-binding cassette transporter A1 (ABCA1) functions as a cholesterol efflux regulatory protein. J Biol Chem 276:23742–23747.

Weers PM, Narayanaswami V, Choy N, Luty R, Hicks L, Kay CM, Ryan RO. 2003. Lipid binding ability of human apolipoprotein E N-terminal domain isoforms: correlation with protein stability? Biophys Chem 100:481–492.

Weisgraber KH. 1990. Apolipoprotein E distribution among human plasma lipoproteins: role of the cysteine–arginine interchange at residue 112. J Lipid Res 31:1503–1511.

Weisgraber KH, Shinto LH. 1991. Identification of the disulfide-linked homodimer of apolipoprotein E3 in plasma. Impact on receptor binding activity. J Biol Chem 266:12029–12034.

Weisgraber KH, Roses AD, Strittmatter WJ. 1994. The role of apolipoprotein E in the nervous system. Curr Opin Lipidol 5:110–116.

Wetterau JR, Aggerbeck LP, Rall SC Jr, Weisgraber KH. 1988. Human apolipoprotein E3 in aqueous solution. I. Evidence for two structural domains. J Biol Chem 263:6240–6248.

Wilson C, Wardell MR, Weisgraber KH, Mahley RW, Agard DA. 1991. Three-dimensional structure of the LDL receptor-binding domain of human apolipoprotein E. Science 252:1817–1822.

Xu Q, Brecht WJ, Weisgraber KH, Mahley RW, Huang Y. 2004. Apolipoprotein E4 domain interaction occurs in living neuronal cells as determined by fluorescence resonance energy transfer. J Biol Chem 279:25511–15516.

Yancey PG, Bielicki JK, Johnson WJ, Lund-Katz S, Palgunachari MN, Anantharamaiah GM, Segrest JP, Phillips MC, Rothblat GH. 1995. Efflux of cellular cholesterol and phospholipid to lipid-free apolipoproteins and class A amphipathic peptides. Biochemistry 34:7955–7965.

THE JOURNAL OF BIOLOGICAL CHEMISTRY VOL. 284, NO. 46, pp. 31914–31920, November 13, 2009

Aβ42-to-Aβ40- and Angiotensin-converting Activities in Different Domains of Angiotensin-converting Enzyme*

Received for publication, April 21, 2009, and in revised form, September 3, 2009 Published, JBC Papers in Press, September 22, 2009, DOI 10.1074/jbc.M109.011437

Kun Zou[‡1], Tomoji Maeda[‡], Atsushi Watanabe[§], Junjun Liu[‡], Shuyu Liu[‡], Ryutaro Oba[¶], Yoh-ichi Satoh[‖], Hiroto Komano[‡2], and Makoto Michikawa[3]**

*From the [‡]Department of Neuroscience, School of Pharmacy, and the [‖]Department of Anatomy, School of Medicine, Iwate Medical University, 2-1-1 Nishitokuda, Yahaba, Iwate 028-3694, Japan, the [¶]Department of Advanced Medicine and Development, BML, Inc., 1361-1 Matoba, Kawagoe, Saitama 350-1101, Japan, and the Departments of [§]Vascular Dementia Research and **Alzheimer Disease Research, National Institute for Longevity Sciences, National Center for Geriatrics and Gerontology, 36-3 Gengo, Morioka, Obu, Aichi 474-8522, Japan*

Amyloid β-protein 1–42 (Aβ42) is believed to play a causative role in the development of Alzheimer disease (AD), although it is a minor part of Aβ. In contrast, Aβ40 is the predominant secreted form of Aβ and recent studies have suggested that Aβ40 has neuroprotective effects and inhibits amyloid deposition. We have reported that angiotensin-converting enzyme (ACE) converts Aβ42 to Aβ40, and its inhibition enhances brain Aβ42 deposition (Zou, K., Yamaguchi, H., Akatsu, H., Sakamoto, T., Ko, M., Mizoguchi, K., Gong, J. S., Yu, W., Yamamoto, T., Kosaka, K., Yanagisawa, K., and Michikawa, M. (2007) *J. Neurosci.* 27, 8628–8635). ACE has two homologous domains, each having a functional active site. In the present study, we identified the domain of ACE, which is responsible for converting Aβ42 to Aβ40. Interestingly, Aβ42-to-Aβ40-converting activity is solely found in the N-domain of ACE and the angiotensin-converting activity is found predominantly in the C-domain of ACE. We also found that the *N*-linked glycosylation is essential for both Aβ42-to-Aβ40- and angiotensin-converting activities and that unglycosylated ACE rapidly degraded. The domain-specific converting activity of ACE suggests that ACE inhibitors could be designed to specifically target the angiotensin-converting C-domain, without inhibiting the Aβ42-to-Aβ40-converting activity of ACE or increasing neurotoxic Aβ42.

Angiotensin-converting enzyme (ACE)[4] plays a key role in the renin-angiotensin system (RAS), which is involved in the long-term regulation of blood pressure and blood volume in the human body. Recent genetic, pathologic, and biochemical studies have associated ACE with onset of Alzheimer disease (AD) (1, 2). The I allele of the *ACE* gene, which results in a reduced serum ACE level, has been demonstrated to be associated with AD (3–5). Hypertension is a risk factor for AD and ACE inhibitors for treatment of hypertension were shown to be the only drug class among the antihypertensives to potentially be associated with a slight increased incidence of AD (adjusted hazard ratio 1.13) (6, 7). A mechanistic link between ACE and AD was suggested when ACE was shown to degrade Aβ40 and Aβ42 (8, 9). Overexpression of Aβ40 in transgenic mice does not cause brain amyloid deposition, the major pathological hallmark of AD, whereas expression of Aβ42 is shown to be essential for amyloid deposition (10, 11). In addition, Aβ40 has an inhibitory effect on amyloid deposition *in vitro* and *in vivo* and has neuroprotective effects (12–14). These lines of evidence suggest that converting Aβ42 to Aβ40 may be a potential strategy for development of an AD therapy. In our previous study, we identified ACE as an Aβ42-to-Aβ40-converting (Aβ-converting) enzyme and showed that ACE inhibitor enhances brain Aβ42 deposition in transgenic mice (15). Clarifying the molecular base of ACE domain-specific enzymatic activity on Aβ42 to Aβ40 conversion, Aβ degradation, and angiotensin conversion emerges to be important for development of a strategy for hypertension and AD treatment.

ACE is a type I integral membrane glycoprotein, and there are two isoforms of ACE in mammals that arise from the use of alternative promoters in a single gene: somatic ACE and testicular ACE. ACE also has one mammalian relative, ACE2, which consists of a single active site domain that, by sequence comparison, more closely resembles the N-domain than the C-domain of somatic ACE. ACE converts angiotensin I to angiotensin II, a potent vasoconstrictor, and inactivates bradykinin, a vasodilator (16). Given the central role ACE plays in regulation of blood pressure, ACE inhibitors are widely used for the treatment of hypertension in the elderly population. ACE also hydrolyzes a wide range of polypeptide substrates, including substance P, luteinizing hormone-releasing hormone, acetyl-Ser-Asp-Lys-Pro (AcSDKP), and neurotensin (16). The mammalian somatic ACE contains two homologous domains, the N-terminal domain (N-domain) and C-terminal domain (C-domain), each bearing a zinc-dependent active site. The pres-

* This work was supported by grants from the Ministry of Education, Culture, Sports, Science and Technology of Japan, Grant-in-Aid for Young Scientists (Start-up) (19800040), and Scientific Research (B) (19300138), the Ministry of Health, Labor and Welfare of Japan (Comprehensive Research on Aging and Health) (H20-007), the Program for Promotion of Fundamental Studies in Health of the National Institute of Biomedical Innovation (NIBIO), Takeda Science Foundation, Kato Memorial Bioscience Foundation, and The Ichiro Kanehara Foundation for the Promotion of Medical Sciences and Medical Care.

[1] To whom correspondence may be addressed. Tel.: 81-19-698-1820; Fax: 81-19-698-1864; E-mail: kunzou@iwate-med.ac.jp.

[2] To whom correspondence may be addressed. Tel.: 81-19-698-1820; Fax: 81-19-698-1864; E-mail: hkomano@iwate-med.ac.jp.

[3] To whom correspondence may be addressed. Tel.: 81-562-46-2311; Fax: 81-562-46-8569; E-mail: michi@nils.go.jp.

[4] The abbreviations used are: ACE, angiotensin-converting enzyme; Aβ, amyloid β-protein; F-ACE, full-domain ACE; N-ACE, N-terminal domain ACE; C-ACE, C-terminal domain ACE; MALDI-TOF-MS, matrix-assisted laser desorption ionization-time of flight-mass spectrometry; AD, Alzheimer Disease.

ence of two active sites in ACE has stimulated many attempts to establish whether they differ in function. For example, AcSDKP, a peptide suggested to inhibit bone marrow maturation, is found to be preferentially cleaved by the N-domain of ACE *in vitro* (17). In contrast, the ACE C-domain is demonstrated to be the main site of angiotensin I cleavage *in vivo* (18). The *N*-linked glycosylation of testicular ACE, a homologue of the somatic ACE N-domain, is essential for its enzymatic activity and for preventing degradation (19).

In our current study, we determined the contributions of each ACE domain, toward Aβ42-to-Aβ40- and/or angiotensin-converting activity. We postulated that the dipeptidyl carboxypeptidase activity of ACE, which converts angiotensin I to angiotensin II and Aβ42 to Aβ40, is located in its C-domain. Surprisingly, we found that the Aβ42-to-Aβ40-converting activity is specifically in the N-domain of ACE, and the angiotensin-converting activity is predominantly in the C-domain of ACE. We also found that both Aβ42-to-Aβ40- and angiotensin-converting activities require the *N*-linked glycosylation of ACE. The finding of domain-specific Aβ42-to-Aβ40-converting activity of ACE may help design a domain-specific ACE inhibitor for treatment of hypertension, without inhibiting the N-domain-specific Aβ42-to-Aβ40-converting activity of ACE.

EXPERIMENTAL PROCEDURES

Truncated ACE Expression and Purification—Expression and purification of ACE recombinant proteins were carried out as described previously (20). Mutated ACE cDNAs containing two active domains (F-ACE) or only the N-terminal active domain or C-terminal active domain (N-ACE or C-ACE) were cloned into pcDNA3.1(-) vectors (Invitrogen). Six histidine residues were introduced at the C-terminal end of each cDNA. The C-terminal transmembrane domain was removed from all of the recombinant ACE proteins to allow them to be secreted into the culture medium. COS7 cells were grown in Dulbecco's modified Eagle's medium (DMEM) containing 10% fetal bovine serum. Transfections of the ACE pcDNA3.1(-) vectors in COS7 cells were performed using Lipofectamine 2000 (Invitrogen), and COS7 cells stably expressing F-, N-, and C-ACE were selected in DMEM containing 10% fetal bovine serum and 1 mg/ml Geneticin (Wako, Japan). Culture media were harvested 3 days after the cells reached confluence, and recombinant ACE proteins were purified using a TALON purification kit (Clontech). The purified proteins were then dialyzed in 50 mM HEPES, 50 mM NaCl, 1 μM $ZnCl_2$, pH 7.5 and concentrated with Centricon YM-50 (Millipore). Protein concentrations of the ACE proteins were determined using a BCA protein assay kit (Pierce).

Western Blot Analysis and Determining Conversion of Aβ42 to Aβ40—COS7 cells were lysed in radioimmune precipitation assay buffer (10 mM Tris/HCl (pH 7.5), 150 mM NaCl, 1% Nonidet P-40, 0.1% sodium dodecyl sulfate (SDS), and 0.2% sodium deoxycholate, containing a protease inhibitor mixture (Roche Applied Science)). The expression of ACE recombinant proteins was detected by Western blotting using a polyclonal anti-ACE antibody (R&D). Aβ1–42 (Peptide Institute) was freshly dissolved in 0.1% $NH_3 \cdot H_2O$ at 200 μM for each experiment. 80 μl of F-, N-, and C-ACE at a concentration of 0.5 μM were mixed with synthetic Aβ42 to a final concentration of 40 μM and incubated at 37 °C. 10 μl of the mixture was subjected to SDS-PAGE and blotted on a nitrocellulose membrane. To enhance the reactivity to an anti-Aβ40 antibody, the membrane was boiled in PBS for 3 min after blotting, probed with an anti-Aβ40 monoclonal antibody (1A10) (IBL), and visualized with SuperSignal (Pierce). Because of the high level of exogenous Aβ42, the membrane was not boiled before the reaction with a polyclonal anti-Aβ42 antibody. The quantitation of Aβ40 generation and Aβ42 degradation was carried out using Image J 1.41 software (NIH).

ACE Activity Assay—F-ACE, N-ACE, and C-ACE were dialyzed in 50 mM HEPES, 50 mM NaCl, 1 μM $ZnCl_2$, pH 7.5, and their activities against the synthetic substrate *N*-hippuryl-l-histidyl-l-leucine (Hip-His-Leu) were determined using an ACE colorimetric kit (Buhlmann Laboratories, Schonenbuch, Switzerland). 10 μl of ACE proteins at a concentration of 0.5 μM were mixed and incubated with ACE substrate at 37 °C. The reaction time was 15 min. All samples were measured in triplicate.

Mass Spectrometry Analysis—Purified F-ACE, N-ACE, or C-ACE was incubated with 80 μM Aβ42 at 37 °C for 2 h. Captopril (10 μM) was added to stop digestion, and the sample was frozen in −80 °C until use. The samples were mixed with 3,5-dimethoxy-4-hydroxycinnamic acid (Wako, Japan) as a matrix, and then subjected to matrix-assisted laser desorption ionization-time of flight-mass spectrometry (MALDI-TOF-MS) (AXIMA-CFR, SHIMADZU, Kyoto, Japan) to detect the generation of Aβ40 and other Aβ fragments. The same amount of F-ACE, N-ACE, C-ACE, or Aβ42 incubated alone under the same conditions as described above was used as control.

Expression of ACE Active Site Mutants and Determining Their Domain-specific Activities—The pcDNA5/FRT expression vectors bearing the catalytically inactive full-length ACE were kindly provided by Dr. Dennis J. Selkoe (9). The two ACE zinc metalloprotease active site glutamates (amino acids 362 in the N-domain and 960 in the C-domain) were changed to aspartates. Mouse embryonic fibroblasts at 90% confluence were transiently transfected with the vectors bearing ACE full-length protein with active site mutations using Lipofectamine 2000 (Invitrogen). After 48 h, the cells were lysed in in 50 mM Tris/HCl (pH 7.5) containing 0.5% Nonidet P-40, and nuclei and cell debris was pelleted at 10,000 × *g* for 10 min at 4 °C. To assay ACE activity, 5 μg of protein of cell lysate was incubated with Hip-His-Leu. For the Aβ42-to-Aβ40-converting activity assay, ACE in each cell lysate was immunoprecipitated using a polyclonal anti-ACE antibody (R&D) and protein G-Sepharose (GE Healthcare). Immunoprecipitated ACE was then incubated with 40 μM synthetic Aβ42 at 37 °C for 15 h. Captopril (10 μM) was added to the mixture to stop the reaction and the conversion of Aβ40 from Aβ42 was detected by Western blot.

Deglycosylation of ACE Proteins—To assess the type of glycosylation of human kidney ACE and recombinant ACE proteins, the ACE proteins were treated with PNGase F, *O*-glycanase, or sialidase A using an enzymatic deglycosylation kit according to the manufacturer's instructions (PROzyme, San Leandro, CA). To evaluate the enzymatic activities of deglycosylated ACE proteins, non-denaturing protocol was used, and ACE proteins

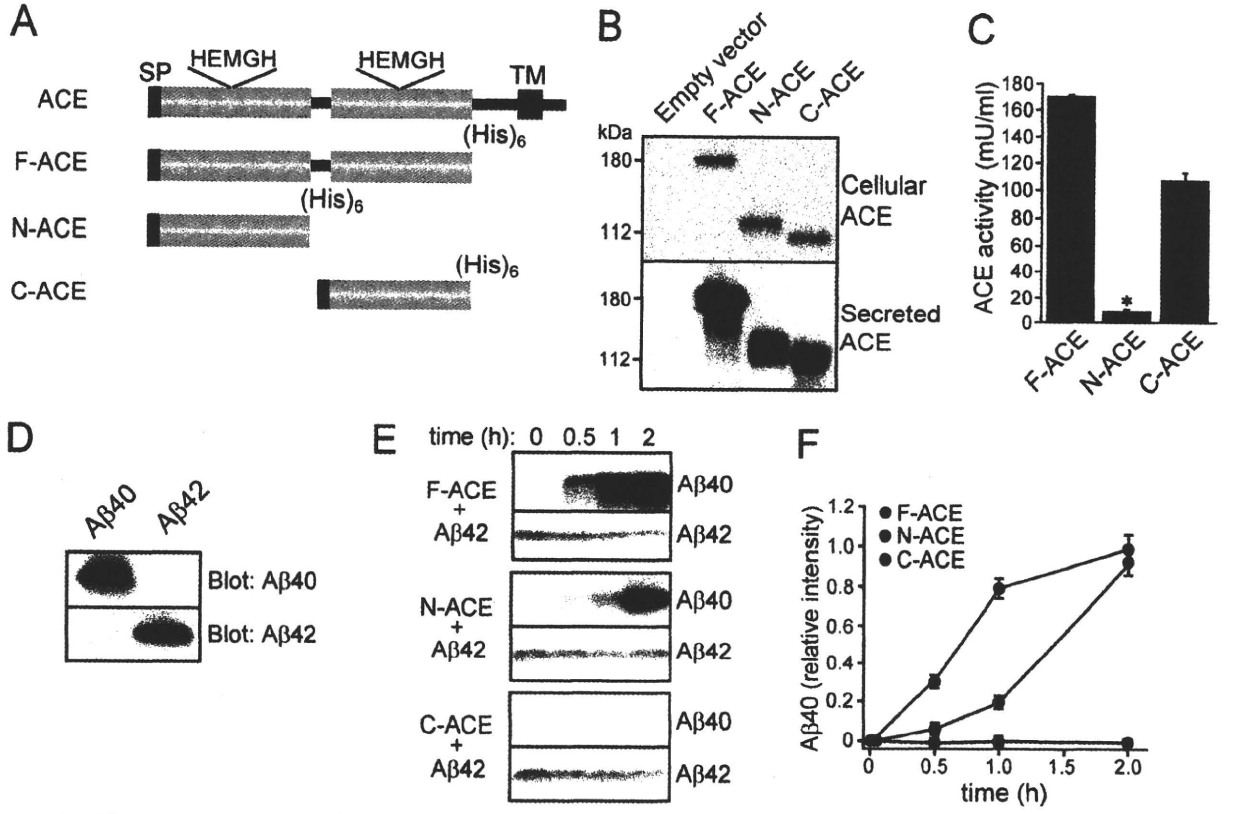

FIGURE 1. **Identification of N-domain-specific Aβ42-to-Aβ40-converting activity of ACE.** *A*, schematic representation of the human ACE and recombinant ACE proteins. The wild-type ACE protein contains a signal peptide (*SP*), a single transmembrane domain (*TM*), and two homologous catalytic domains (*light blue box*). Recombinant ACE proteins, F-ACE, N-ACE, and C-ACE, contain 6 histidine residues (*yellow box*) at the C terminus and a signal peptide at the N terminus. *B*, COS7 cells transfected with empty vector or cells stably expressing F-ACE, N-ACE, or C-ACE were lysed in radioimmune precipitation assay buffer. Western blots of 20 μg of total protein from the cells or 2 μg of ACE isolated from the culture medium were probed with a polyclonal anti-ACE antibody. *C*, ACE activity was measured by incubating 0.5 μM F-ACE, N-ACE, or C-ACE with the substrate Hip-His-Leu for 15 min at 37 °C. N-ACE has markedly reduced ACE activity compared with C-ACE. Values represent the means + S.E.; $n = 3$; *, $p < 0.001$, Bonferroni/Dunn test. *D*, specificities of monoclonal anti-Aβ40 (1A10) and polyclonal anti-Aβ42 antibodies were confirmed by Western blot of 0.1 μg of Aβ40 and Aβ42. *E*, F-, N-, and C-ACE were mixed with synthetic Aβ42 and incubated at 37 °C for 0.5, 1, or 2 h. Western blots of the mixture were probed with anti-Aβ40 and anti-Aβ42 antibodies. In contrast to the ACE activity, the Aβ42-to-Aβ40-converting activity was solely detected in N-ACE. *F*, generation of Aβ40 and the degradation of Aβ42 were determined by densitometry.

were deglycosylated at 37 °C for 1 h. The non-deglycosylated ACE proteins were mixed with the same incubation buffer provided by the manufacturer and incubated except that glycosidases were not added.

RESULTS

ACE N-domain, but Not C-domain, Converts Aβ42 to Aβ40—To explore which domain of ACE has Aβ42-to-Aβ40-converting activity, we prepared 3 kinds of recombinant ACE proteins, which were transfected into COS7 cells. F-ACE contains both the N-domain and C-domain active sites. N-ACE contains only the N-terminal active site, and C-ACE only contains the C-terminal active site. All three kinds of mutated ACE were fused with a 6-histidine tag at the C-terminal for the isolation from the culture medium (Fig. 1*A*). Cell lines stably expressing F-ACE, N-ACE, or C-ACE were selected by Geneticin and the expression of the ACE-mutated proteins were confirmed by Western blot. The endogenous ACE was not detected in the cell lysate of COS7 cells transfected with empty vectors. F-, N-, and C-ACE showed molecular masses at 180, 130, and 110 kDa, respectively (Fig. 1*B*). The secreted ACE recombinant proteins were isolated from the culture medium by immobilized metal chromatography. The proteins were then dialyzed and concentrated. The apparent molecular mass of each secreted ACE recombinant protein did not differ from each of the cellular ACE recombinant proteins (Fig. 1*B*). ACE enzymatic activity of the F-ACE, N-ACE, and C-ACE was confirmed by degradation of the substrate Hip-His-Leu (Fig. 1*C*). F-ACE was found to have the highest Hip-His-Leu-degrading activity and C-ACE had 63% ACE activity compared with F-ACE, whereas N-ACE had a significantly reduced ACE activity, confirming the finding of the ACE C-domain as the main site of angiotensin I cleavage *in vivo* (18) (Fig. 1*C*).

We have found that ACE releases two amino acids from the C terminus of Aβ42 and generates Aβ40. Aβ1–41 was not found during the degradation of Aβ42 by ACE, suggesting that the Aβ42-to-Aβ40-converting activity of ACE is a dipeptidyl carboxypeptidase enzymatic activity (15). To determine which domain is responsible for the Aβ42-to-Aβ40-converting activity, we incubated Aβ42 with F-ACE, N-ACE, or C-ACE and examined the generation of Aβ40 from Aβ42 by Western blot using anti-Aβ40- and anti-Aβ42-specific antibodies. The specificity of the two antibodies was examined by Western blotting of synthetic Aβ40 and Aβ42, and cross reaction between these

two antibodies was not found (Fig. 1*D*). Unexpectedly, in contrast to the angiotensin-converting activity, the Aβ42-to-Aβ40-converting activity was found in F-ACE and N-ACE, but not in C-ACE, indicating that N-domain of ACE has the Aβ42-to-Aβ40-converting activity. Although C-ACE showed a similar Aβ42-degrading activity compared with F-ACE and N-ACE, it did not generate Aβ40 from Aβ42 (Fig. 1*E*). Incubation of C-ACE with Aβ42 up until 16 h did not generate Aβ40 (data not shown). F-ACE generated more Aβ40 from Aβ42 than N-ACE at the time points of 0.5 and 1 h, whereas at the time point of 2 h F-ACE and N-ACE generated similar amounts of Aβ40 (Fig. 1, *E* and *F*). F-ACE had similar activities compared with native human kidney ACE regarding the Aβ42-to-Aβ40-converting activity and the Hip-His-Leu-degrading activity (Figs. 1*E* and 4*C* and data not shown).

To determine other products other than Aβ40 that were generated by ACE from Aβ42 and to confirm the result from Western blot, we performed mass spectrometry analysis. Consistent with our immunological studies, a peak corresponding to Aβ1–40 was detected in the F-ACE- and N-ACE-digested samples; in addition, F-ACE and N-ACE also generated peaks corresponding to Aβ1–33, Aβ1–28, Aβ1–24, and Aβ1–21 from Aβ42, whereas Aβ1–40 was not formed by C-ACE. However, C-ACE generated four other Aβ fragments, Aβ1–33, Aβ1–28, Aβ1–24, and Aβ1–21 (Fig. 2*A*). Mass spectrometry analysis for incubated F-ACE, N-ACE, or C-ACE alone did not show any Aβ peptide signal, and synthetic Aβ42 only showed one peak with a mass at 4514, which matched the predicted mass of Aβ1–42 (Fig. 2*B* and data not shown). These results from mass spectrometry confirmed that the Aβ42-to-Aβ40-converting activity is restricted to the ACE N-domain.

N-domain-inactive ACE Mutant Loses Aβ42-to-Aβ40-converting Activity—Three ACE mutants were generated by site-directed mutagenesis to change the active site sequence HEMGH to HDMGH in N-, C-, or both N- and C-domain. The N-domain active site was inactivated by mutating glutamate 362 to aspartate (termed E362D), and the C-domain active site was similarly inactivated by mutating glutamate 960 to aspartate (termed E960D). E362/960D has double mutations in its N- and C-domain active sites (Fig. 3*A*). The fibroblasts were transiently transfected with empty vector or ACE mutant constructs. ACE was not detected in the fibroblasts transfected with empty vector, and wtACE and ACE mutants were expressed in the cells at a similar level (Fig. 3*B*). To determine the effects of each ACE active site on ACE activity, cell lysate from each cell lines was analyzed for ACE activity. Consistent with our results from purified truncated ACE proteins, E362D containing only the C-domain active site has the similar ACE activity compared with wtACE, whereas E960D has an extremely low ACE activity. ACE inhibitor, captopril, completely inhibited this ACE activity (Fig. 3*C*). To determine which active site in each domain is responsible for the Aβ42-to-Aβ40-converting activity, wtACE and ACE mutant proteins were immunoprecipitated and incubated with Aβ42. A similar amount of immunoprecipitated ACE was confirmed by Western blotting (Fig. 3*D*, *upper panel*). E960D without the C-domain activity generated similar amount of Aβ40 from Aβ42 compared with

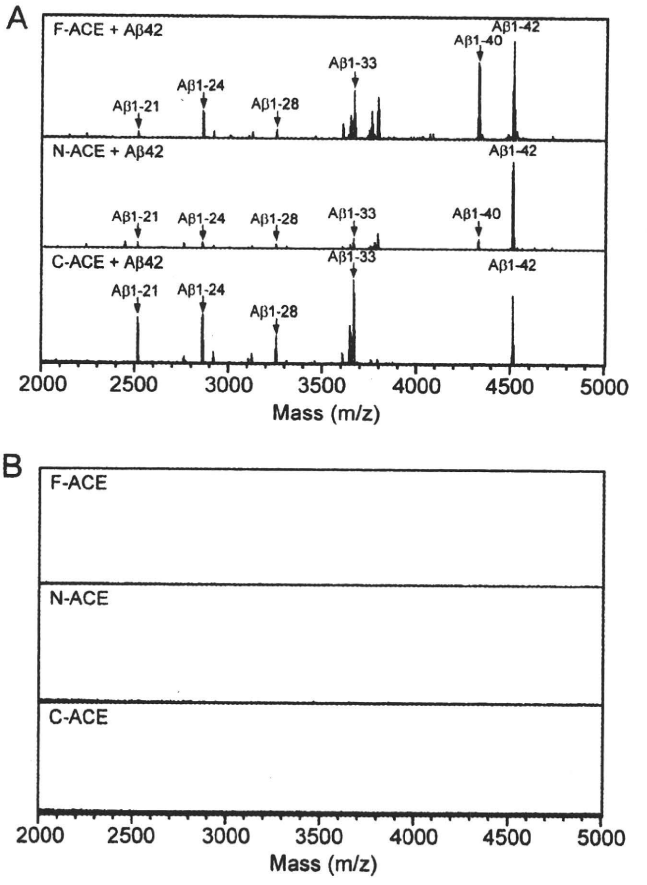

FIGURE 2. **MALDI-TOF-MS analysis for Aβ42 degradation by F-ACE, N-ACE, or C-ACE.** *A*, Aβ42 (80 μM) was incubated with 0.5 μM purified F-ACE, N-ACE, or C-ACE at 37 °C for 2 h, then captopril (10 μM) was added after incubation to stop the digestion. 1 μl of the mixture was subjected to MALDI-TOF-MS analysis. F-ACE and N-ACE generated Aβ1–40, whereas C-ACE did not. *B*, 1 μl of F-ACE, N-ACE, or C-ACE alone incubated at 37 °C for 2 h was subjected to MALDI-TOF-MS analysis, and a peptide signal was not detected.

wtACE, whereas E362D and E362/960D without N-domain activity did not convert Aβ42 to Aβ40 (Fig. 3*D*, *middle panel*).

N-Glycosylation Is Essential for Aβ42-to-Aβ40- and Angiotensin-converting Activities—ACE is a glycoprotein, and the *N*-linked glycosylation of testicular ACE has been shown to be essential for its angiotensin-converting activity. Human ACE has 17 putative Asn*X*(Ser/Thr) *N*-linked glycosylation sites distributed throughout both the N-domain and C-domain (21). To determine the role of glycosylation of ACE in its enzymatic activities and to compare the glycosylation of natural human ACE with that of recombinant F-ACE, N-ACE, and C-ACE, we examined the type of glycosylation of these ACE proteins by the treatment with PNGase F, *O*-glycanase, and sialidase A. Treatment with PNGase F, *O*-glycanase, and sialidase A remarkably reduced the molecular weight of human kidney ACE, F-ACE, N-ACE, and C-ACE (Fig. 4*A*, *lanes 1* and *2*). Removal of *N*-linked glycosylation using PNGase F alone produced similar molecular weight shifts, whereas *O*-glycanase did not produce any shift in ACE size (Fig. 4*A*, *lanes 3* and *4*). The sensitivity of N-ACE to PNGase F indicates that N-ACE is modified by *N*-linked glycosylation. All the ACE proteins showed a slight decrease in the molecular weight after sialidase A digestion,

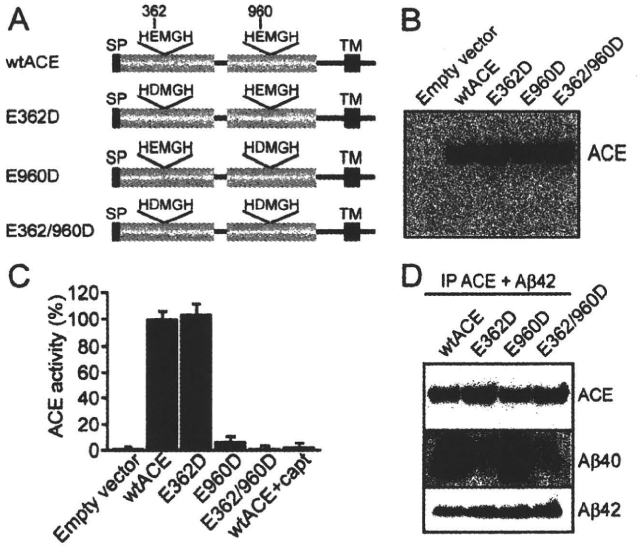

FIGURE 3. **Site-directed mutated ACE proteins exhibit domain-specific Aβ42-to-Aβ40- and angiotensin-converting activity.** *A*, schematic representation of human ACE and the mutant positions. The two ACE zinc metalloprotease active site glutamates (amino acids 362 in the N-domain and 960 in the C-domain) were changed to aspartates. *B*, fibroblasts were transiently transfected with empty vector, wtACE or mutant ACE plasmids and the expression of ACE proteins was detected by Western blotting using a polyclonal anti-ACE antibody. *C*, ACE activity was measured by incubating 5 μg of protein of cell lysate with the substrate Hip-His-Leu for 10 min at 37 °C. ACE activity in cell lysate was clearly detected in wtACE and E362D. C-domain inactive ACE protein, E960D, showed an extremely low ACE activity; and double mutants in both domains of ACE, E362/960D, did not show ACE activity. ACE activity was clearly inhibited by captopril (1 μM) treatment. *D*, ACE in cell lysate (4 mg of protein) from each transfected cell line was immunoprecipitated by 5 μg of polyclonal anti-ACE antibody and 100 μl of protein G-Sepharose. Immunoprecipitated ACE was then incubated with synthetic Aβ42 and the generation of Aβ40 was detected by Western blotting. *SP*, signal peptide; *TM*, transmembrane.

indicating the sialylation of their *N*-glycans (Fig. 4*A*, *lane 5*). These results suggest that the glycosylation type of natural human kidney ACE and recombinant ACE proteins produced by COS7 cells are identical. Because ACE is modified by *N*-linked glycosylation and *O*-linked glycosylation was not detected, we used PNGase to remove its *N*-glycans and studied the ACE activity. As expected, PNGase-treated human kidney ACE showed a 96% reduced ACE activity in degradation of Hip-His-Leu compared with untreated ACE (Fig. 4*B*).

To determine the role of *N*-linked glycosylation of ACE in its Aβ42-to-Aβ40-converting activity, we incubated Aβ42 with PNGase F-treated or untreated human kidney ACE and examined Aβ40 generation by Western blot. Deglycosylated human kidney ACE showed a decreased molecular mass at ~150 kDa and was degraded by itself after 2 h of incubation. After incubation for 16 h, ~150-kDa deglycosylated ACE was completely degraded (Fig. 4*C*, *upper panel*). Aβ40 was generated from Aβ42 by ACE after incubating the mixture of Aβ42 and ACE for 15 min. The level of Aβ40 increased in a time-dependent manner and reached a peak after incubation for 2 h, whereas deglycosylated ACE did not generate Aβ40 from Aβ42, although it showed a similar Aβ42-degrading activity compared with non-deglycosylated ACE (Fig. 4*C*, *middle and bottom panels*). This glycosylation-required Aβ42-to-Aβ40-converting activity was also confirmed in recombinant ACE proteins. PNGase F-deglycosylated F-ACE, N-ACE, and C-ACE have similar Aβ42-degrading activity. However, deglycosylated F-ACE and N-ACE failed to generate Aβ40 from Aβ42, suggesting that the *N*-linked glycosylation in the ACE N-domain is essential for its Aβ42-to-Aβ40-converting activity (Fig. 4*D*). Sialidase A treatment did not change the Aβ42-to-Aβ40-converting activity and the ACE activity of human kidney ACE, indicating that sialylation is not required for its activities (data not shown).

Captopril and Enalaprilat Showed Different IC_{50} on Aβ42-to-Aβ40-converting Activity—The feature of ACE inhibitors has been well studied in terms of their angiotensin-converting inhibitory effect. To explore whether ACE inhibitors differentially inhibit the Aβ42-to-Aβ40-converting activity, we determined the IC_{50} of captopril, perindopril, lisinopril, and enalaprilat toward the angiotensin- and Aβ42-to-Aβ40-converting activity of F-ACE. All four ACE inhibitors showed a similar IC_{50} on the inhibition of angiotensin-converting activity of F-ACE, whereas enalaprilat exhibited a 10-fold lower IC_{50} (0.003~0.01 μM) on Aβ42-to-Aβ40-converting activity than captopril (0.03~0.1 μM) (Table 1).

DISCUSSION

Most mammalian tissues contain ACE with two catalytic domains. Evolutionary conservation of the ACE N- and C-domains suggests important distinct functions of these domains. Recent genetic studies have associated the I allele of the *ACE* gene, which results in a reduced serum ACE level, with onset of AD (1, 3). We have shown previously that ACE converts Aβ42 to Aβ40, and its inhibition predominantly enhances brain Aβ42 deposition (15). To investigate which domain of ACE is responsible for Aβ42-to-Aβ40-converting activity and whether ACE inhibitors inhibit this activity, we generated three kinds of ACE proteins, containing both N- and C-domains or containing either single active domain. We also used selective site-directed mutagenesis of ACE to study the domain-specific activity of full-length ACE. The present study shows that the Aβ42-to-Aβ40- and angiotensin-converting activities were located in different ACE domains and that *N*-linked glycosylation was essential for the two ACE enzymatic activities. The N-domain of ACE clearly showed an Aβ42-to-Aβ40-converting activity, whereas it has an extremely low angiotensin-converting activity. In contrast, the C-domain of ACE showed angiotensin-converting activity, whereas the Aβ42-to-Aβ40-converting activity was not detected in this domain.

In a cellular context, both the N-domain and C-domains of ACE are able to degrade Aβ40 and Aβ42 (9). In our studies, we also found that the N- and C-domains were indistinguishable as regarding degrading Aβ42, suggesting that both N- and C-domains of ACE have endopeptidase activity for Aβ42. In the overall scheme of Aβ42 processing, the full-length ACE cleaving into many fragments may be important for therapeutic treatment of AD. We showed that Aβ40, but not Aβ41, was generated from Aβ42 (Fig. 2*A*). However, the Aβ42-to-Aβ40-converting activity was solely found in the N-domain of ACE (Figs. 1, 2, and 3). These results suggest that the dipeptidyl carboxypeptidase activity converting Aβ42 to Aβ40 is restricted to its N-domain. The N-domain specific dipeptidyl activity was

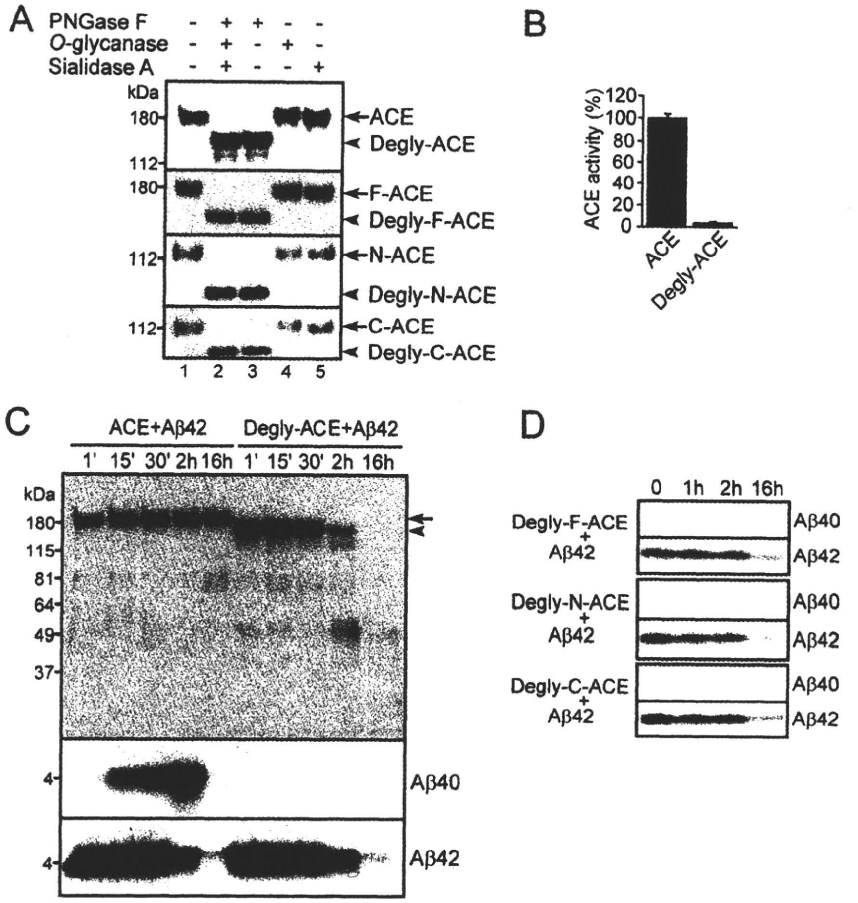

FIGURE 4. **Characterization of ACE glycosylation and role of the glycosylation in ACE activity and Aβ42-to-Aβ40-converting activity.** *A*, 5 μg of purified human kidney ACE, F-ACE, N-ACE, and C-ACE were deglycosylated with 1 μl of PNGase F, *O*-glycanase, and/or sialidase A for 1 h at 37 °C. PNGase F alone was able to remove all glycosylation of ACE. *B*, ACE activity of PNGase F-deglycosylated human kidney ACE was measured immediately after deglycosylation using an ACE colorimetric kit. ACE activity was almost completely abolished by *N*-deglycosylation. *C*, 80 μl of human kidney ACE (0.5 μM) with or without *N*-deglycosylation was mixed with synthetic Aβ42 (40 μM) and incubated at 37 °C. 10 μl of the mixture were collected at various incubation time points and subjected to Western blot analysis. Deglycosylated ACE showed no Aβ42-to-Aβ40-converting activity, whereas the Aβ42-degrading activity remained. *D*, 40 μl of recombinant F-, N-, and C-ACE proteins (0.5 μM) were deglycosylated and mixed with Aβ42 and incubated at 37 °C for 1, 2, or 16 h. Aβ42-to-Aβ40-converting activity was not detected in either deglycosylated F-ACE or deglycosylated N-ACE, whereas all the deglycosylated ACE showed an Aβ42-degrading activity.

TABLE 1

ACE inhibitors inhibited Aβ42-to-Aβ40-converting activity with different IC_{50}

ACE activity of 10 μl of F-ACE (0.5 μM) was measured using an ACE colorimetric kit, and Aβ42-to-Aβ40-converting activity was measured by Western blotting and densitometry. 0, 0.003, 0.01, 0.03, 0.1, 0.3, 1, 3, 10 μM ACE inhibitors were added to determine the IC_{50} for Aβ42-to-Aβ40-converting activity.

ACE inhibitors	ACE activity IC_{50}	Aβ-converting activity IC_{50}[a]
	μM	μM
Captopril	0.01–0.03	0.03–0.1
Enalaprilat	0.01–0.03	0.003–0.01
Lisinopril	0.01–0.03	0.01–0.03
Perindopril	0.03–0.1	0.01–0.03

[a] Aβ-converting activity, Aβ42-to-Aβ40-converting activity.

also found in the degradation of AcSDKP, which is involved in the control of hematopoietic stem cell proliferation. The molecular basis in which the N-domain of ACE accesses AcSDKP and Aβ42 remains to be elucidated. The N- and C-domains of ACE have reduced Aβ42-to-Aβ40-converting activity and angiotensin-converting activity, respectively, compared with full domain ACE (Fig. 1, *C* and *F*), suggesting that each catalytic domain of ACE regulates the activity of the other, and both domains are required for normal substrate recognition and degradation. Mice with a selective inactivation of either the N- or C-domain of ACE were generated, and the C-domain was demonstrated to be the main site of angiotensin I cleavage (18, 22), which is consistent with our *in vitro* finding. However, the role of the N-domain of ACE toward Aβ42 to Aβ40 conversion *in vivo* needs to be addressed.

It has been previously reported that testicular ACE, the C-domain isoform of ACE, without *N*-linked glycosylation has no enzyme activity and was rapidly degraded (19). We confirmed that deglycosylation of human kidney ACE abolished its angiotensin-converting activity, whereas the endopeptidase activity for degrading itself and Aβ42 was not affected. Moreover, the N-domain-specific Aβ42-to-Aβ40-converting activity was abolished by the deglycosylation, indicating that the *N*-linked glycosylation is also essential for maintaining the N-domain-specific enzymatic activity of ACE. Deglycosylated ACE was retained as an intact protein 30 min after deglycosylation. ACE activity and Aβ42-to-Aβ40-converting activity were clearly detected in non-deglycosylated ACE within 30 min (Fig. 4, *B* and *C*). Thus, the loss of ACE activity and Aβ42-to-Aβ40-converting activity of deglycosylated ACE may not result from its self-degradation, but likely result from the deglycosylation. These results suggest that *N*-linked glycosylation is required to maintain the ACE structure and its dipeptidyl carboxypeptidase activity in both N- and C-domains. Presenilins have been shown to be involved in the maturation of membrane proteins, whether presenilin mutants in familial AD affect ACE glycosylation and its Aβ42-to-Aβ40-converting activity need to be clarified in future (23). Finally, we showed that ACE inhibitors inhibited the N-domain-specific Aβ42-to-Aβ40-converting activity each with a different IC_{50}. Among the examined ACE inhibitors, enalaprilat has the strongest inhibitory effect on Aβ42-to-Aβ40-converting activity. This result may provide a mechanism underlying the finding that non-centrally active ACE inhibitors, such as enalapril, are associated with a greater risk of incident dementia (24). In

our previous *in vivo* study, captopril treatment enhanced predominantly brain Aβ42 deposition in 17-month-old amyloid precursor protein (APP) transgenic mice and led to a tendency of increased brain Aβ42/40 ratio (15). Taking the anti-amyloid and antioxidant effects of Aβ40 into account, our findings suggest that ACE inhibitors could be designed specifically to target the C-domain of ACE without inhibiting its N-domain-specific Aβ42-to-Aβ40-converting activity.

Acknowledgments—We thank Dr. Dennis J. Selkoe for providing wtACE, E362D, E960D, and E362/960D plasmids and thank Dr. Paul Langman for English correction.

REFERENCES

1. Kehoe, P. G., and Wilcock, G. K. (2007) *Lancet Neurol.* **6,** 373–378
2. Zou, K., and Michikawa, M. (2008) *Rev. Neurosci.* **19,** 203–212
3. Lehmann, D. J., Cortina-Borja, M., Warden, D. R., Smith, A. D., Sleegers, K., Prince, J. A., van Duijn, C. M., and Kehoe, P. G. (2005) *Am. J. Epidemiol.* **162,** 305–317
4. Kehoe, P. G., Russ, C., McIlory, S., Williams, H., Holmans, P., Holmes, C., Liolitsa, D., Vahidassr, D., Powell, J., McGleenon, B., Liddell, M., Plomin, R., Dynan, K., Williams, N., Neal, J., Cairns, N. J., Wilcock, G., Passmore, P., Lovestone, S., Williams, J., and Owen, M. J. (1999) *Nat. Genet.* **21,** 71–72
5. Elkins, J. S., Douglas, V. C., and Johnston, S. C. (2004) *Neurology* **62,** 363–368
6. Skoog, I., Lernfelt, B., Landahl, S., Palmertz, B., Andreasson, L. A., Nilsson, L., Persson, G., Odén, A., and Svanborg, A. (1996) *Lancet* **347,** 1141–1145
7. Khachaturian, A. S., Zandi, P. P., Lyketsos, C. G., Hayden, K. M., Skoog, I., Norton, M. C., Tschanz, J. T., Mayer, L. S., Welsh-Bohmer, K. A., and Breitner, J. C. (2006) *Arch. Neurol.* **63,** 686–692
8. Hu, J., Igarashi, A., Kamata, M., and Nakagawa, H. (2001) *J. Biol. Chem.* **276,** 47863–47868
9. Hemming, M. L., and Selkoe, D. J. (2005) *J. Biol. Chem.* **280,** 37644–37650
10. Mucke, L., Masliah, E., Yu, G. Q., Mallory, M., Rockenstein, E. M., Tatsuno, G., Hu, K., Kholodenko, D., Johnson-Wood, K., and McConlogue, L. (2000) *J. Neurosci.* **20,** 4050–4058
11. McGowan, E., Pickford, F., Kim, J., Onstead, L., Eriksen, J., Yu, C., Skipper, L., Murphy, M. P., Beard, J., Das, P., Jansen, K., Delucia, M., Lin, W. L., Dolios, G., Wang, R., Eckman, C. B., Dickson, D. W., Hutton, M., Hardy, J., and Golde, T. (2005) *Neuron* **47,** 191–199
12. Zou, K., Gong, J. S., Yanagisawa, K., and Michikawa, M. (2002) *J. Neurosci.* **22,** 4833–4841
13. Zou, K., Kim, D., Kakio, A., Byun, K., Gong, J. S., Kim, J., Kim, M., Sawamura, N., Nishimoto, S., Matsuzaki, K., Lee, B., Yanagisawa, K., and Michikawa, M. (2003) *J. Neurochem.* **87,** 609–619
14. Kim, J., Onstead, L., Randle, S., Price, R., Smithson, L., Zwizinski, C., Dickson, D. W., Golde, T., and McGowan, E. (2007) *J. Neurosci.* **27,** 627–633
15. Zou, K., Yamaguchi, H., Akatsu, H., Sakamoto, T., Ko, M., Mizoguchi, K., Gong, J. S., Yu, W., Yamamoto, T., Kosaka, K., Yanagisawa, K., and Michikawa, M. (2007) *J. Neurosci.* **27,** 8628–8635
16. Turner, A. J., and Hooper, N. M. (2002) *Trends Pharmacol. Sci.* **23,** 177–183
17. Rousseau, A., Michaud, A., Chauvet, M. T., Lenfant, M., and Corvol, P. (1995) *J. Biol. Chem.* **270,** 3656–3661
18. Fuchs, S., Xiao, H. D., Hubert, C., Michaud, A., Campbell, D. J., Adams, J. W., Capecchi, M. R., Corvol, P., and Bernstein, K. E. (2008) *Hypertension* **51,** 267–274
19. Sadhukhan, R., and Sen, I. (1996) *J. Biol. Chem.* **271,** 6429–6434
20. Oba, R., Igarashi, A., Kamata, M., Nagata, K., Takano, S., and Nakagawa, H. (2005) *Eur. J. Neurosci.* **21,** 733–740
21. Soubrier, F., Alhenc-Gelas, F., Hubert, C., Allegrini, J., John, M., Tregear, G., and Corvol, P. (1988) *Proc. Natl. Acad. Sci. U.S.A.* **85,** 9386–9390
22. Fuchs, S., Xiao, H. D., Cole, J. M., Adams, J. W., Frenzel, K., Michaud, A., Zhao, H., Keshelava, G., Capecchi, M. R., Corvol, P., and Bernstein, K. E. (2004) *J. Biol. Chem.* **279,** 15946–15953
23. Zou, K., Hosono, T., Nakamura, T., Shiraishi, H., Maeda, T., Komano, H., Yanagisawa, K., and Michikawa, M. (2008) *Biochemistry* **47,** 3370–3378
24. Sink, K. M., Leng, X., Williamson, J., Kritchevsky, S. B., Yaffe, K., Kuller, L., Yasar, S., Atkinson, H., Robbins, M., Psaty, B., and Goff, D. C., Jr. (2009) *Arch. Intern. Med.* **169,** 1195–1202

Neurobiology of Disease

A Noncompetitive BACE1 Inhibitor TAK-070 Ameliorates Aβ Pathology and Behavioral Deficits in a Mouse Model of Alzheimer's Disease

Hiroaki Fukumoto,[1]* Hideki Takahashi,[1]* Naoki Tarui,[1] Junji Matsui,[1] Taisuke Tomita,[2] Mitsuhiro Hirode,[1] Masumi Sagayama,[1] Ryouta Maeda,[1] Makiko Kawamoto,[1] Kazuko Hirai,[1] Jun Terauchi,[1] Yasufumi Sakura,[1] Mitsuru Kakihana,[1] Kaneyoshi Kato,[1] Takeshi Iwatsubo,[2,3] and Masaomi Miyamoto[1]

[1]Pharmaceutical Research Division, Takeda Pharmaceutical Company Limited, Yodogawa-ku, Osaka 532-8686, Japan, and [2]Department of Neuropathology and Neuroscience, Graduate School of Pharmaceutical Sciences, and [3]Department of Neuropathology, Graduate School of Medicine, The University of Tokyo, Bunkyo-ku, Tokyo 113-0033, Japan

We discovered a nonpeptidic compound, TAK-070, that inhibited BACE1, a rate-limiting protease for the generation of Aβ peptides that are considered causative for Alzheimer's disease (AD), in a noncompetitive manner. TAK-070 bound to full-length BACE1, but not to truncated BACE1 lacking the transmembrane domain. Short-term oral administration of TAK-070 decreased the brain levels of soluble Aβ, increased that of neurotrophic sAPPα by ~20%, and normalized the behavioral impairments in cognitive tests in Tg2576 mice, an APP transgenic mouse model of AD. Six-month chronic treatment decreased cerebral Aβ deposition by ~60%, preserving the pharmacological efficacy on soluble Aβ and sAPPα levels. These results support the feasibility of BACE1 inhibition with a noncompetitive inhibitor as disease-modifying as well as symptomatic therapy for AD.

Introduction

The accumulation of amyloid-β peptides (Aβ) in the brain is strongly implicated in the pathogenesis of Alzheimer's disease (AD), and considered as a prime target for the disease-modifying therapy of AD (Selkoe and Schenk, 2003). Aβ is proteolytically produced through sequential cleavages by β- and γ-secretases from amyloid precursor protein (APP). The β-secretase cleavage of APP is executed by a membrane-bound aspartic protease, β-site APP-cleaving enzyme 1 (BACE1), which is considered to be the rate-limiting step in the production of Aβ (Cole and Vassar, 2008), whereas a majority of APP is cleaved by α-secretase at the midportion of Aβ sequence in a way to preclude Aβ production, by competing with BACE1.

γ-Secretase generates the C termini of Aβ with different length, e.g., $Aβ_{40}$ or $Aβ_{42}$, the latter being considered as the pathogenic species (Iwatsubo et al., 1994). Inhibition of γ-secretase may potentially cause side effects, because genetic knock-out (KO) of presenilin 1 and 2, the catalytic subunits of γ-secretase, leads to embryonic lethality due to failure in activation of Notch, which is essential for development and differentiation (Shen et al., 1997; Wong et al., 1997; Donoviel et al., 1999). Furthermore, cognitive deficits associated with synaptic degeneration have been documented in PS1/PS2 conditional KO mice with or without APP transgenic background (Saura et al., 2004, 2005; Chen et al., 2008). In contrast, BACE1 KO mice do not show such fatal phenotypes despite its complete ablation, except for partial hypomyelination at the developmental stage (Hu et al., 2006; Sankaranarayanan et al., 2008) or schizophrenia-like behavior in homozygous BACE1 KO mice (Savonenko et al., 2008), whereas cognitive deficits are ameliorated on APP transgenic background (Ohno et al., 2004, 2006, 2007). Furthermore, it has been well documented that the protein levels or activities of BACE1 are upregulated in the brains of patients with sporadic AD (Stockley and O'Neill, 2007). Therefore, BACE1 is considered as a promising target for the mechanism-based therapy for AD. So far, several BACE1 inhibitors have been reported (Hussain et al., 2007; Sankaranarayanan et al., 2009; Silvestri, 2009), although no compound that is orally active and highly penetrable to brain tissues with functional ameliorations has been documented.

We conducted a cell-based assay in the IMR32 human neuroblastoma cell line for small chemical compounds that reduce the secretion of Aβ and increase that of sAPPα, the latter being recognized as neurotrophic with ameliorative effects on cognitive behaviors (Isacson et al., 2002; Postina, 2008). Finally we discovered a nonpeptidic compound, (*R*)-6-[(1,1′-biphenyl)-4-ylmethoxy]-1,2,3,4-tetrahydro-*N*,*N*-dimethyl-2-naphthalene-ethan-amine hydrochloride·monohydrate (TAK-070) (Fig. 1), as a novel noncompetitive BACE1 inhibitor. TAK-070 ameliorated Aβ pathology and behavioral deficits in Tg2576, an APP transgenic model mice of AD, although the reduction in Aβ levels was modest,

Received June 7, 2010; accepted June 30, 2010.

We thank the Mayo Clinic for supplying the Tg2576 mice, Kozo Shimakawa for breeding the Tg2576 mice, Satoko Osawa for technical assistance, Dr. Gopal Thinakaran for valuable advice, and Drs. Zen-ichi Terashita, Yasuhiro Sumino, and Shigenori Ohkawa for continuous support to the study.

*H.F. and H.T. contributed equally to this work.

All authors except for T. Tomita and T. Iwatsubo are employees of Takeda Pharmaceutical Company, which was engaged in the research of BACE1 inhibitors for potential use as AD therapeutics.

Correspondence should be addressed to Dr. Hiroaki Fukumoto, Pharmaceutical Research Division, Takeda Pharmaceutical Company Limited, 2-17-85 Juso-honmachi, Yodogawa-ku, Osaka 532-8686, Japan. E-mail: Fukumoto_Hiroaki@takeda.co.jp.

DOI:10.1523/JNEUROSCI.2884-10.2010

 0270-6474/10/3011157-10$15.00/0

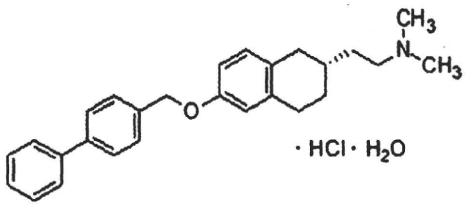

Figure 1. Chemical structure of TAK-070.

unlike those observed by complete ablation of BACE1. We propose that the partial reduction in Aβ as well as increase in sAPPα by a noncompetitive BACE1 inhibition may be sufficient to modify amyloid pathology and ameliorate cognitive deficits, without causing potential adverse events by complete BACE1 ablation.

Materials and Methods

Compound

The chemical TAK-070 was made by Takeda Pharmaceutical Company Limited (Takeda), and the chemical structure is shown in Figure 1. The chemical synthesis and related information are described in the patent of JP-A 11-80098 (*WO98/38156*). γ-Secretase inhibitor IX (DAPT) was purchased from Calbiochem.

Cell cultures and sample preparation

IMR32 human neuroblastoma cell line was obtained from American Type Culture Collection (ATCC), and mouse Neuro-2a neuroblastoma cells stably expressing human Swedish mutant APP (N2aAPPsw cells) were generated as described previously (Tomita et al., 2002). For ELISA analysis, cells were cultured on 48-well multi-plates at 5×10^4 cells/cm^2 to reach near total confluence in DMEM (Nikken Biomedical Laboratory) supplemented with 10% (v/v) heat-inactivated fetal bovine serum (FBS) (Wako) in a humid atmosphere containing 10% CO_2. The culture medium was replaced with DMEM/0.2% bovine serum albumin (BSA) (Wako) containing various concentrations of TAK-070, and the cells were cultured for 24 h. The conditioned media were subjected to ELISA quantitation.

Quantitation of sAPPα and Aβ by ELISA

To quantitate human sAPPα, we used LN27 that recognizes the N-terminal portion of APP (Zymed) as a capture antibody. ELISA plates (high binding, clear plate, Greiner) were filled with LN27 (0.5 μg/ml, 75 μl/well) in carbonated buffer (100 mmol/L, pH 9.6) and incubated at 4°C overnight. After washing the plates with PBS (Invitrogen) three times, each well was blocked with 100 μl of BlockAce solution (Dai-Nippon) diluted fourfold (v/v) for >2 h. After washing the plates with PBS twice, 50 μl samples or standards prepared from conditioned media containing sAPPα were mixed with 50 μl of buffer A (20 mmol/L phosphate buffer, pH 7.2, 10% BlockAce, 0.2% protease-free BSA, 0.05% thimerosal, 0.4 mol/L NaCl, 0.076% CHAPS, 2 mmol/L EDTA-2Na, 0.2% SDS, and 4 mmol/L DTT) in each well. Buffer A contains DTT to break the S-S bond of sAPPα to enhance the recognition by the LN27 antibody. The mixture was incubated in the plate overnight at 4°C. After washing the plates with PBS four times, BAN50-HRP (75 μl/well) [which recognizes the C-terminal portion of human sAPPα (Asami-Odaka et al., 1995)] diluted in the detection buffer (20 mmol/L phosphate buffer, pH 7.2, 1% protease-free BSA, 2 mmol/L EDTA-2Na, 0.05% thimerosal, and 0.4 mol/L NaCl) was added to each well. The plates were incubated at room temperature for 3–4 h. After washing the plates with PBS six times, substrates were added and the reaction mixtures were developed. To measure sAPPα in brain lysates, the homogenate buffer free of detergents was used to preclude contamination of membrane-associated APP.

$A\beta_{40}$ or $A\beta_{42}$ was quantitated by two-site sandwich ELISA using a capture antibody BNT77, which recognizes the midportion of Aβ without detecting $A\beta_{17\text{-}40/42}$ (i.e., the cleaved products by α- and γ-secretases) (Fukumoto et al., 1999), and the detector antibodies of BA27-HRP or BC05-HRP that specifically detect the C termini of $A\beta_{40}$ or $A\beta_{42}$, respectively, as described previously (Asami-Odaka et al., 1995). TMB substrate (Pierce) was used as a chromogenic substrate. After stopping the reaction with phosphoric acid solution (1 mol/L, 75 μl/well), the enzymatic products were measured using a multi-label counter at OD450 (WALLAC Arvo Sx; PerkinElmer Life Sciences).

Immunoblot analysis

Quantification of the levels of sAPPβ, sAPPα, APP, APP C-terminal fragment (CTF) (e.g., C83 and C99), BACE, or ADAM10 was performed on conditioned media or cell lysates of N2aAPPsw cells treated with vehicle DMSO (0.1% v/v), 3 μmol/L TAK-070, or 3 μmol/L DAPT for 24 h. SeeBlue Plus2 (Invitrogen) was used as a molecular weight standard. Protein samples separated by SDS-PAGE were electrophoretically transferred to an Immobilon PVDF membrane (Millipore). The membranes were blocked with 5% (w/v) skim milk solution (Wako) in TBS-T (20 mmol/L Tris-buffer, pH 7.0, containing 50 mmol/L NaCl and 0.1% Tween 20) and reacted overnight with a detector antibody. The following monoclonal or polyclonal antibodies were used: monoclonal antibodies that specifically react with the C terminus of Swedish mutant sAPPβ (sAPPβsw) [clone 6A1, IBL, 1:100 dilution (Lakshmana et al., 2009)], the C terminus of human sAPPα [BAN50, Takeda, 0.5 μg/ml (Asami-Odaka et al., 1995)], α-tubulin (clone AA4.3, Developmental Studies Hybridoma Bank, cultured medium from hybridoma), respectively, and polyclonal antibodies to the C terminus of APP [APP(C), No. 18961; IBL, 1:1000 dilution] that detect total APP and APP-CTFs, anti-mouse/rat APP [APP(597), No. 28055; IBL, 1:1000 dilution] raised against the C-terminal 16 aa of rodent sAPPα that specifically recognizes rodent, but not human, sAPPα, anti-sAPPβ [No. 18957; IBL, 1:100 dilution (Lakshmana et al., 2009)] specific for sAPPβ derived from wild-type APP (sAPPβwt), ADAM10 (735–749) (No. 422751; Calbiochem, 0.5 μg/ml), and the C terminus of BACE1 (No. 28051; IBL, 0.1 μg/ml, 1:200). Specificity of anti-human/mouse APP antibodies is shown in supplemental Figure S1 (available at www.jneurosci.org as supplemental material). The hybridoma clone AA4.3 was obtained from the Developmental Studies Hybridoma Bank developed under the auspices of the National Institute of Child Health and Human Development and maintained by The University of Iowa, Department of Biology (Iowa City, IA). After washing with TBS-T, the membranes were further incubated with TBS (20 mmol/L Tris-buffer, pH 7.0, containing 50 mmol/L NaCl) buffer containing an anti-mouse IgG antibody-HRP (1/5000) for a monoclonal antibody or an anti-rabbit IgG antibody-HRP (1/5000) (GE Healthcare) for polyclonal antibodies. The membranes were washed with TBS-T, and then immunoreactive bands were visualized using Immunostar, Immunostar LD (Wako), or SuperSignal West Femto Maximum Sensitivity Substrate (Thermo Scientific) according to the manufacturer's instructions. The intensity of bands on the membrane was captured and quantitated using LAS-1000plus (FUJIFILM).

Cell-based assay for α-secretase activity

The assay (Doedens et al., 2003) was performed with a slight modification. N2aAPPsw cells were cultured in DMEM supplemented with 10% FCS until grown to confluence. The cells were collected by PBS (−) (Ca^{2+}, Mg^{2+} free) buffer and centrifuged for 5 min at 300 × *g*. After washing with PBS (−), the cells were suspended in PBS (−) at a final concentration of 4×10^7 cells/ml. The enzymatic reaction was initiated by combining an equal volume (100 μl) of cell suspension and reaction mixture at a final cell concentration of 2×10^7 cells/ml, 10 μmol/L each of leupeptin (Peptide Institute), aprotinin (Roche Diagnostics), and α-secretase fluorogenic substrate [MCA-HQKLVFFA (K-DNP), BioSource], with vehicle of DMSO, TAK-070 (final concentration: 3 μmol/L), or (−)-epigallocatechin-3-gallate (catechin, Wako) (final concentration: 20 μmol/L). After each incubation time point, the cells were centrifuged, the cell-free supernatants of each 100 μl were added to a 96-well black plate (Greiner), and fluorescence intensity after cleavage by α-secretase was measured (excitation 320 nm, emission 400 nm) (WALLAC Arvo Sx; PerkinElmer Life Sciences).

Expression and purification of FLAG-tagged full-length BACE1 or truncated BACE1 (1-454)

The plasmid containing cDNA encoding the entire coding frame of human BACE1 (clone No. FG04087) was obtained from KAZUSA DNA Research

Institute. The full-length BACE1 (1-501) and C-terminally truncated BACE1 (1-454, 460, 465, 471 and 474) lacking the transmembrane domain were cloned into pcDNA3.1 (−) (Invitrogen) vector with a C-terminal FLAG tag [pcDNA3.1(−)BACE1-flag and pcDNA3.1(−)BACE1(1-454, 460, 465, 471, or 474)-flag, respectively]. COS-7 cells were cultured in DMEM supplemented with 10% (v/v) heat-inactivated FBS at 37°C in a humid atmosphere of 5% CO_2. Cells were grown in an F225 cell culture flask (225 cm^2) and transfected with 22.5 μg of pcDNA3.1(−)BACE1-flag or pcDNA3.1(−)BACE1(1-454, 460, 465, 471, or 474)-flag, using Fugene6 (Roche Diagnostics). Forty-eight hours after transfection, cells were scraped in PBS and centrifuged for 10 min at 1870 × *g*. The supernatant was used as a source for further purification of the truncated BACE1 (1-454, 460, or 465). To purify full-length BACE1 or truncated BACE1 (1-471 or 474), the pellet was resuspended in 50 mmol/L Tris-HCl buffer, pH 7.4, containing 0.15 mol/L NaCl, 1 mmol/L EDTA, and 0.1 mmol/L PMSF. The cells were disrupted by sonication and centrifuged at 1870 × *g* for 10 min. The supernatant was centrifuged at 100,000 × *g* for 45 min to yield crude membrane pellets. The membrane was solubilized in 50 mmol/L Tris-HCl buffer, pH 7.4, containing 50 mmol/L octyl-β-glucoside, 0.15 mol/L NaCl, 1 mmol/L EDTA, and 0.1 mmol/L PMSF at 4°C for 2 h, centrifuged at 100,000 × *g* for 45 min. The fractions containing full-length of BACE1, C-terminally truncated BACE1 (1-454, 460, 465, 471, or 474) fused with FLAG tag were then loaded on an Anti-FLAG M2 affinity gel (Sigma) column. The column was washed with 50 mmol/L Tris-HCl buffer, pH 7.4, containing 0.15 mol/L NaCl, and purified FLAG-tagged recombinant BACE1 proteins were obtained by elution with 100 μg/ml FLAG peptides.

Cell-free assay for BACE1 activity

A statine substrate analog inhibitor PI (TEEISEVNXVAEF; X = statine) (Sinha et al., 1999) and the fluorogenic substrate for BACE1 [Nma-SEVKMDAEK(Dnp)RR-NH_2] were purchased from the Peptide Institute. The substrate was dissolved in 125 mmol/L acetic acid. TAK-070 and PI were dissolved in dimethylformamide (DMF). Assays were performed in black 96-well microplates (Greiner) in a final volume of 50 μl. Each well contained 25 μl of acetate buffer (pH 5.5, 50 mmol/L), 10 μl of recombinant BACE1, 10 μl of substrate (250 μmol/L), and 5 μl of various concentrations of compounds at a final DMF concentration of 0.5%. The assay mixtures were incubated at 37°C for 20 h. After incubation, the fluorescence of the enzymatic product was measured at 460 nm (excitation at 325 nm) using Fluoroskan Ascent (Labsystems). The percentage of inhibition was calculated by an equation of 100 × [1 − (test − blank)/(control − blank)], where test, control, and blank are fluorescence intensities in the presence of a compound, absence of a compound, and absence of both the BACE1 enzyme and a compound, respectively. IC_{35} values were calculated by linear regression analysis using a BSAS program. To clarify the inhibition profile, double-reciprocal (Lineweaver–Burk) plot analysis was performed using 10 μl substrate of 100, 150, 250, 500, or 1000 μmol/L (a final concentration of 20, 30, 50, 100, or 200 μmol/L, respectively) and 5 μl of TAK-070 of 100 or 300 μmol/L (a final concentration of 10 or 30 μmol/L) in total assay solution of 50 μl. The reciprocal of change in the fluorescence value in the presence of TAK-070 at each concentration was plotted on the vertical axis, and the reciprocal of the substrate concentration was plotted on the longitudinal axis.

Surface plasmon resonance binding assay

We used a Biacore3000/BiacoreA100 instrument to generate sensorgrams for binding of TAK-070 onto full-length BACE1, C-terminally truncated BACE1 (1-454), (1-460), (1-465), (1-471), (1-474), APP688 [Leu18-Leu688 with a C-terminal 6-His tag, also referred to as protease nexin II containing Kunitz-type Protease Inhibitor (KPI) domain, #3466-PI, R&D Systems], and sAPPβ containing KPI domain (BACE1-cleaved N-terminal product of APP, #SIG-39938, Sigma). Each protein was immobilized on a Sensor Chip CM5 (carboxymethylated dextran matrix chip) using amine-coupling kit (Biacore). The sensorgrams were recorded at a flow rate of 30 μl/60 s in a solution of PBS containing 10% DMSO and 0.005% Surfactant P20 (Biacore) at room temperature. TAK-070 was initially dissolved in DMSO and diluted in PBS containing 0.005% Surfactant P20 at a final concentration of 0.5–8, 5, or 10 μmol/L. Specific binding to each protein was calculated as signal to each protein subtracted by signal to vehicle (DMSO).

Animals

All animals were housed in rooms maintained at 24°C with a 12 h light/dark cycle. Food (chow containing TAK-070; Oriental Yeast) and tap water were provided *ad libitum*. In each experiment, mice were randomly grouped, avoiding differences in body weight among groups. All experiments using animals were reviewed and approved by the Internal Animal Care and Use Committee of Takeda Pharmaceutical Research Laboratories.

Short-term treatment of Tg2576 by TAK-070

Female Tg2576 mice at 2 months of age were used for short-term treatment with TAK-070. Tg2576 were fed either chow containing TAK-070 (5.6 ppm or 56 ppm, corresponding to ~0.87 or 8.2 mg/kg, p.o., respectively; $n = 15$) or chow without TAK-070 ($n = 15$) for 7 weeks. Then, each mouse was decapitated and the cerebral cortex was dissected out on ice. Each sample was immediately frozen on dry ice and stored at −80°C until assay. Halves of the cerebral cortices were homogenized in ice-cold Tris-extraction buffer (50 mmol/L Tris, pH 7.2, 200 mmol/L sodium chloride, 2% protease-free bovine serum albumin, and 0.01% thimerosal) containing protease inhibitor cocktails (1 mmol/L PMSF, 40 KIU aprotinin, 10 μmol/L pepstatin A, 1 mmol/L phosphoramidon, 10 mmol/L 1,10-phenanthroline, 2 mmol/L EDTA) without detergents. After centrifugation at 21,000 × *g* for 5 min, the supernatants were further diluted and subjected to sandwich ELISAs for $A\beta_{40}$, $A\beta_{42}$, or sAPPα.

Long-term treatment of Tg2576 by TAK-070

Male and female Tg2576 mice at 7 months of age ($n = 16–17$ for each group, $n = 8–9$, male; $n = 8$, female) were used for long-term treatment with TAK-070. Tg2576 mice were fed chow containing TAK-070 (56 ppm, corresponding to ~7 mg/kg/d, p.o., when evaluated at 6 months of treatment) for 6 months and a week from 7 months of age, or chow without TAK-070 (vehicle control). Male Tg2576 mice at 8 months of age ($n = 9$) were used as a young control. After decapitation, the brains were removed and the left cerebral hemisphere was immediately frozen on dry ice and stored at −80°C until biochemical assays; the right hemisphere was fixed in 4% paraformaldehyde for 24 h, embedded in paraffin, and subjected to immunohistochemical analysis. Biochemical quantitation of Aβ and sAPPα was performed as follows: the cerebral cortex was initially homogenized with ice-cold Tris-extraction buffer and centrifuged as in the short-term treatment study to obtain the supernatants for quantitation of soluble Aβ and sAPPα. The pellet was then homogenized in a 19-fold volume of ice-cold 70% formic acid, and centrifuged at 44,000 × *g* for 5 min. The supernatant was further diluted, neutralized with 1 mol/L Tris-based solution, and the levels of insoluble $A\beta_{40}$ and $A\beta_{42}$ were quantitated by ELISA.

Immunohistochemistry

Immunohistopathological analysis was performed on two distinct coronal sections from the right hemisphere at the level of the hippocampus and thalamus of Tg2576 mice. Sample preparation and quantitation of Aβ plaques were conducted under blinded conditions for the examiner. Four-micrometer-thick sections were deparaffinized and pretreated with 99% formic acid for 5 min. The section was blocked with 10% fetal calf serum for 30 min and then reacted with BAN50 (0.5 μg/ml) at 4°C overnight. BAN50-positive plaques were visualized with Dako REAL EnVision Detection Kit (Dako) using diaminobenzidine as a chromogen. The amyloid burden with a diameter more than ~30 μm (percentage of immunopositive areas that comprised the total area) and the number of plaques throughout the right cerebral neocortices were quantitated using Vanox (AH-2, Olympus) connected to a digital video camera (Prog Res 3012, Carl Zeiss) and image analysis software (Win ROOF, Mitani).

Y-maze and Morris water maze tests

Male Tg2576 mice of 18 weeks of age were divided into three groups, i.e., vehicle-treated ($n = 14$), TAK-070 1 mg/kg treated ($n = 14$), and TAK-070 3 mg/kg treated ($n = 14$). Wild-type littermates ($n = 15$) were used

as a nontransgenic control group. Tg2576 mice were treated with TAK-070 (1 or 3 mg/kg, p.o.) or vehicle (0.5% methylcellulose; MC) once a day for 9 d before the behavioral test. Each mouse was treated with drugs after all trials were completed every day during the test period. Each mouse was sequentially subjected to Y-maze test on day 10, and then in Morris water maze test from day 11 to day 13. On day 14, the mice were decapitated. The brains were dissected out on ice immediately and stored at −80°C.

Y-maze test. To measure spontaneous alternation behavior and exploratory activity, a black Y-maze with arms of 40 cm length, 3 cm width, with 12.5 cm walls was used. Each animal underwent one trial, during which the animal was placed into one of the three alleys and allowed free exploration of the maze for 5 min, and alternations and total numbers of arm choices were recorded. Spontaneous alternation, expressed as a percentage, refers to ratio of arm choices differing from the previous two choices to the total number of arm entries.

Morris water maze test. The water maze pool comprised a circular plastic water tank, 120 cm in diameter and 20 cm in depth. The pool was filled with water at room temperature to a height of 15 cm. A transparent acrylic platform (10 × 10 cm), its top surface being 0.5 cm below the surface of water, was located in a constant position in the middle of one quadrant from the center and edge of the pool, and was invisible for mice inside the pool. Each mouse was given four trials daily for 3 consecutive days with an interval of ~20 min. The sequence of the starting points was randomly selected. The escape latency and the swimming distance for mice to find the hidden platform were automatically recorded by the computer analyzing system (Target/2, Neuroscience). The value for each session was defined as the mean of four trials. The probe test was not conducted because the deficits were too modest to evaluate the effects of compounds.

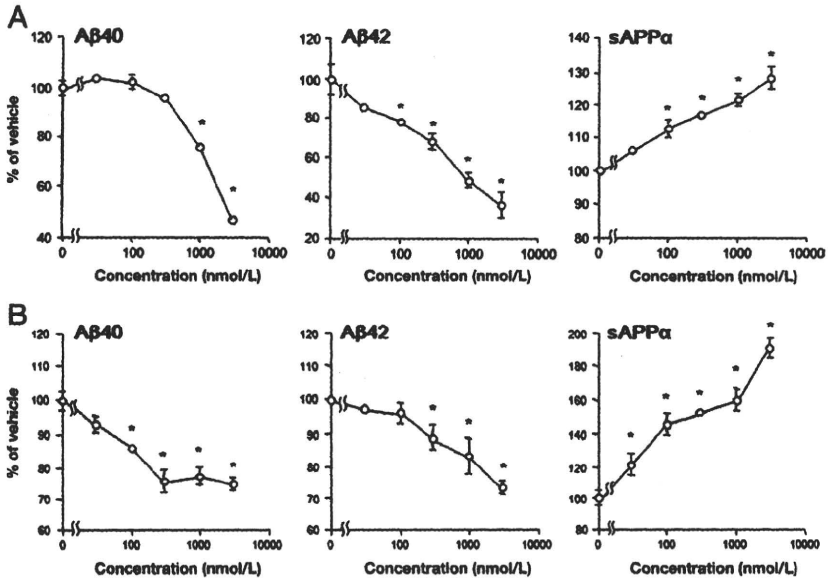

Figure 2. Effects of TAK-070 on secretion of Aβ and sAPPα in cultured cells. The levels of $Aβ_{40}$, $Aβ_{42}$, and sAPPα secreted in conditioned media were quantitated by ELISAs. ***A***, Human IMR32 neuroblastoma cells were treated with TAK-070 for 24 h. Vehicle control levels for $Aβ_{40}$ and $Aβ_{42}$ were 17.3 and 5.8 fmol/ml on average, respectively. Levels of sAPPα were determined as arbitrary unit values. Values are mean percentages relative to levels in the control (±SEM) in four independent experiments. ***B***, Mouse Neuro2a neuroblastoma cells stably expressing human APPsw (N2aAPPsw cells) were treated with TAK-070 for 24 h. Vehicle control levels of $Aβ_{40}$ and $Aβ_{42}$ were 447.6 and 114.6 fmol/ml, respectively. Levels of sAPPα were determined as arbitrary unit values. Values are mean percentages of the control (±SEM) in six independent experiments. *$p < 0.025$, compared with the vehicle control (one-tailed Williams' test).

Novel object recognition test

Male Tg2576 mice of 5 months of age were divided into two groups, vehicle treated ($n = 14$) and TAK-070 3 mg/kg treated ($n = 15$). As a nontransgenic control group, wild-type littermates ($n = 15$) were used. Tg2576 mice were treated with TAK-070 (3 mg/kg, p.o.) or vehicle (0.5% MC) once a day for 15 d before the test. During the test, each mouse was treated with TAK-070 or vehicle after all trials were completed.

Each mouse was subjected to the novel object recognition test from day 16 to day 17. In the acquisition session on day 16, the same two objects were placed in the back corner of the test box (30 × 30 × 30 cm). The mouse was then placed in another corner of the box and the time exploring each object was recorded for 5 min. After 24 h later on day 17, animals were placed back into the same box, except that one of the familiar objects used during the acquisition was replaced with a novel object. The animals were then allowed to explore freely for 5 min. A preference ratio of the time exploring the novel object to the time exploring both objects was calculated as an index of cognitive function.

Statistical analysis

Statistical analysis was performed by the one-tailed Williams' test for analysis of multiple groups in dose–response study, by Tukey's test for analysis of multiple groups in no dose–response study or Student's *t* test for analysis of two groups under the BSAS program.

Results

TAK-070 reduced Aβ secretion and increased that of sAPPα in cell cultures

We treated human IMR-32 neuroblastoma cells with TAK-070 for 24 h, and measured the levels of Aβ and sAPPα in the conditioned media by ELISA. We observed a concentration-dependent suppression of the secretion of Aβ, with minimum effective concentrations (MECs) for $Aβ_{40}$ and $Aβ_{42}$ of ~100 and ~1000 nmol/L, respectively (Fig. 2*A*). TAK-070 also stimulated sAPPα production in a concentration-dependent manner with MEC of ~100 nmol/L. The percentage reduction in the levels of $Aβ_{40}$ and $Aβ_{42}$, and percentage increase in that of sAPPα by treatment with 3 μmol/L TAK-070 were ~50, ~70, and ~30%, respectively. Similarly significant effects at submicromolar to micromolar ranges of TAK-070 on APP processing (~25% reduction in Aβ secretion and ~90% increase in sAPPα at 3 μmol/L TAK-070) were observed in mouse Neuro-2a neuroblastoma cells stably overexpressing human APP carrying Swedish-type familial Alzheimer mutation (APPsw; N2aAPPsw cells) (Fig. 2*B*).

TAK-070 inhibited BACE1 activity in cultured cells

We next examined the effects of TAK-070 in N2aAPPsw cells by immunoblot analysis. Treatment with TAK-070 (3 μmol/L) significantly decreased the secreted level of both human Swedish sAPPβ and mouse endogenous sAPPβ, N-terminal counterparts of APP generated by BACE1 cleavage, by ~16 and ~19%, respectively. Simultaneously, the levels of human and mouse endogenous sAPPα were increased by ~70% and ~30%, respectively (Fig. 3*A*). We then examined the effects of TAK-070 on the levels of membrane-bound APP and its C-terminal stubs (e.g., C83 and C99), BACE1, and ADAM10 [a neuronal α-secretase candidate (Jorissen et al., 2010)] in lysates of N2aAPPsw cells. TAK-070 decreased the level of C99 by ~15%, in contrast to the prominent

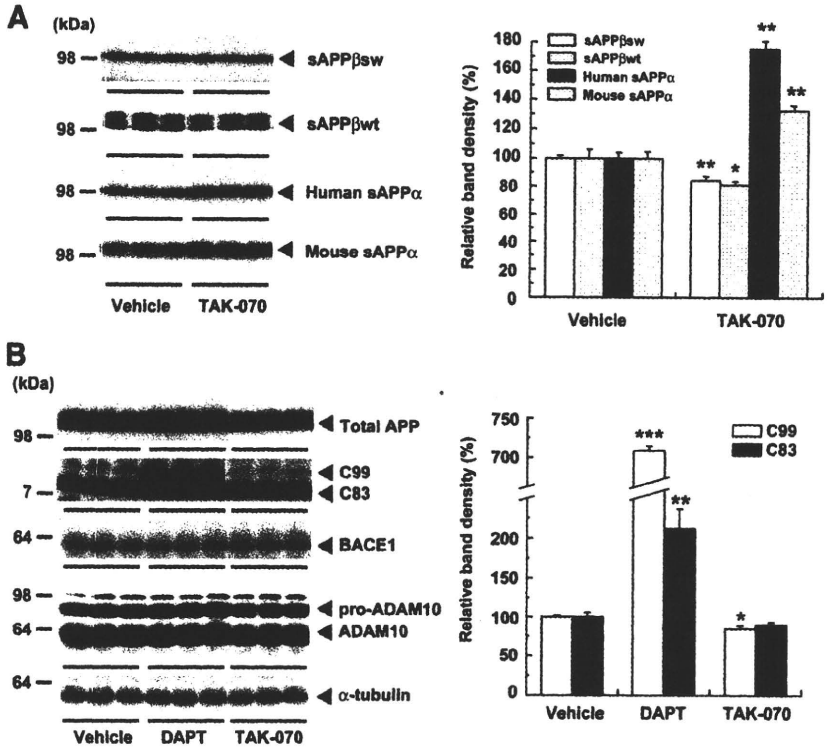

Figure 3. Immunoblot analysis of the protein levels of APP derivatives and those of secretases in N2aAPPsw cells. *A*, Immunoblots of sAPPβ (sAPPβsw derived from transfected human APPsw and sAPPβwt from endogenous mouse APP) and sAPPα (human sAPPα derived from transfected human APPsw and mouse sAPPα from endogenous APP) in media after treatment with TAK-070 (3 μmol/L) or vehicle from three independent experiments are shown. Values in the graph (right) show the mean percentages of band intensities analyzed by densitometry relative to those in vehicle control ($\pm$SEM) in the three independent experiments. $^*p < 0.05$, $^{**}p < 0.01$, versus vehicle control (Student's *t* test). *B*, Immunoblots of APP, C-terminal fragments of APP (C99 and C83), BACE1 and high- and low-molecular-weight forms of ADAM10 (pro- and matured forms, respectively) from lysates of N2aAPPsw cells treated with vehicle, DAPT (3 μmol/L), or TAK-070 (3 μmol/L) are shown. Levels of α-tubulin are shown as an internal control. Note that all the immunoblot data are obtained from a single membrane replica with identical exposure. Values for C99 and C83 (right) are mean percentages of band intensities analyzed by densitometry relative to those in vehicle control ($\pm$SEM) in the three independent experiments. $^*p < 0.05$, $^{**}p < 0.01$, $^{***}p < 0.001$, versus vehicle control (Student's *t* test).

increase in the levels of C83 and C99 (by ~2.1- and ~7.1-fold, respectively) by inhibition of γ-secretase by DAPT (Fig. 3*B*). TAK-070 treatment did not significantly affect the protein levels of APP, C83, BACE1, or ADAM10 (Fig. 3*B*). The levels of mouse sAPPβ in the conditioned media of TAK-070-treated naive N2a cells also was decreased (supplemental Fig. S1, available at www.jneurosci.org as supplemental material). We further examined the effects of TAK-070 on α-secretase activity using a cell-based, peptide cleavage assay (Doedens et al., 2003). Although (−)-epigallocatechin-3-gallate induced the enzymatic activity, in line with the reported increase in the active form of ADAM10 (Obregon et al., 2006), TAK-070 did not show any incremental effects on the α-secretase-cleaved product (supplemental Fig. S2, available at www.jneurosci.org as supplemental material), suggesting that TAK-070 is not an α-secretase activator.

Noncompetitive BACE1 inhibition by TAK-070 in a cell-free assay

To confirm that TAK-070 has a direct inhibitory effect on BACE1, we developed a cell-free assay, using recombinant full-length human BACE1 and a quenching type fluorogenic BACE1 substrate based on ~10 aa residues flanking the β-cleavage site of wild-type human APP. TAK-070 inhibited the BACE1 activity in a concentration-dependent manner, with IC_{35} of ~3.15 μmol/L and MEC of ~100 nmol/L (Fig. 4*A*), the latter being a similar effective concentration to that in cell culture studies (Fig. 2*A*,*B*). Under the same experimental conditions, a peptidic BACE1 inhibitor (TEEISEVNXVAEF; X = statine) inhibited BACE1 activity with IC_{35} value of 38.8 nmol/L, which was consistent with the previously published data (Sinha et al., 1999). To further examine the inhibitory profile of TAK-070, we conducted a Lineweaver–Burk plot analysis by incubating the fluorogenic BACE1 substrate with recombinant full-length human BACE1 in the presence of 10 or 30 μmol/L TAK-070. All fitted lines converged at an identical point on the *x*-axis with an estimated K_m value of 156 μmol/L (Fig. 4*B*), indicating that TAK-070 inhibits BACE1 in a noncompetitive manner. The K_i value estimated from the *y*-axis values with an intercept of $(1 + [I]/K_i)/V_{max}$ was 19 μmol/L.

TAK-070 did not inhibit other aspartic proteases (e.g., cathepsin D and E, renin, and γ-secretase (Takahashi et al., 2003)), nor activated enzymatic activity of human TACE in cell-free assays even at the concentration of 100 μmol/L (data not shown), in agreement with the cell culture data described above.

Binding of TAK-070 to full-length BACE1, but not to its extracellular domain

To gain further insight into the mechanism of the noncompetitive BACE1 inhibition by TAK-070, we examined the binding of TAK-070 to BACE1 using a surface plasmon resonance assay. Since TAK-070 inhibited the proteolytic activity of full-length BACE1 [BACE1 (1-501)] in a noncompetitive manner, but not that of the truncated BACE1 (1-454), lacking the transmembrane domain (data not shown), we first compared the binding of TAK-070 to BACE1 (1-501) or truncated BACE1 (1-454). Surface Plasmon resonance assay clearly showed that TAK-070 was specifically bound to BACE1 (1-501) in a concentration-dependent manner (0.5–8 μmol/L), but not to BACE1 (1-454) within the same concentration range (Fig. 5*A*). To further narrow down the binding site of TAK-070 within the C-terminal region of BACE1, we examined the binding of TAK-070 to a series of C-terminally truncated BACE1, i.e., BACE1 (1-460), (1-465), (1-471), and (1-474). The binding of TAK-070 to BACE1 (1-460) and (1-465) was completely lost, whereas BACE1 (1-474) retained a comparable affinity to TAK-070 as BACE1 (1-501), and the binding of BACE1 (1-471) was partially impaired (Fig. 5*B*). These data suggest that the critical region within the C terminus of BACE1 for binding to TAK-070 resides around residues 465-474, a subdomain of the membrane spanning region. We also examined the binding of TAK-070 to recombinant proteins of APP (18-688) containing Kunitz-type protease inhibitor domain and the BACE1-cleavage site or sAPPβ, and found that neither APP (18-688) nor sAPPβ showed significant binding to TAK-070 (5

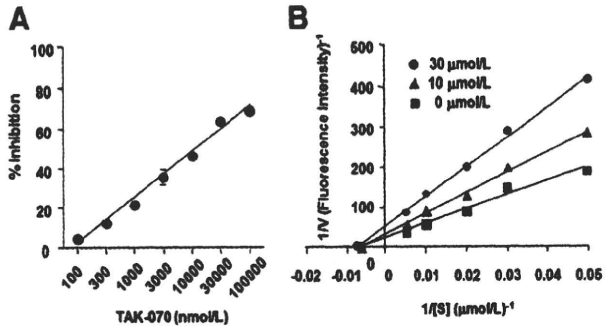

Figure 4. Noncompetitive inhibition of BACE1 activity by TAK-070 in cell-free assay. ***A***, Concentration-dependent inhibition of BACE1 activity by TAK-070. Human recombinant full-length BACE1 purified from COS-7 cells (rhBACE1) was incubated with a fluorogenic BACE1 substrate based on the amino acid sequence of wild-type human APP flanking the BACE1 cleavage site (Nma-SEVKMDAEK(Dnp)RR-NH2) in the presence of various concentrations of TAK-070 (indicated in abscissa, in nanomoles per liter). Values are mean percentage inhibition (±SEM) in three independent experiments. ***B***, Lineweaver–Burk plot analysis of the mode of inhibition by TAK-070. rhBACE1 was incubated with 20–200 μmol/L BACE1 substrate in the presence (10 or 30 μmol/L) or absence of TAK-070. The plots of 1/*V* versus 1/[S] were fitted by the Lineweaver–Burk straight line. Result of a representative experiment is shown.

μmol/L) (supplemental Fig. S3, available at www.jneurosci.org as supplemental material).

These data from cell-based and cell-free studies collectively indicate that TAK-070 is a direct, noncompetitive inhibitor for BACE1 that acts by binding to the noncatalytic site of BACE1, presumably to the transmembrane domain.

TAK-070 reduced Aβ and increased sAPPα in the brains of Tg2576 mice

We then examined whether TAK-070 is effective on Aβ and sAPPα in the brains of Tg2576 mice, a transgenic mouse model of AD that overexpresses APPsw. We first performed a short-term treatment, feeding young female Tg2576 mice with chow containing TAK-070 (5.6 and 56 ppm, corresponding to 0.87 and 8.2 mg/kg/d, p.o., respectively) starting at 2 months of age for 7 weeks. All mice survived without any differences in body weight and food consumption among cohorts. Oral administration of TAK-070 significantly reduced the levels of soluble $A\beta_{40}$ and $A\beta_{42}$ in Tris buffer-soluble fractions of the cerebral cortex (average ± SEM: 7707 ± 334 and 1825 ± 100 fmol/g wet weight, respectively, in vehicle group) by ~16–23%, and increased that of sAPPα by ~15–21% at both doses (Fig. 6*A*).

We next conducted a long-term treatment of Tg2576 mice with TAK-070. We started treatment at the age of ~7 months, just before Tg2576 mice develop the Aβ deposition as amyloid plaques (at ~8 months). Tg2576 mice were fed with chow containing 56 ppm TAK-070 until 13 months of age for ~6 months. Tg2576 mice tolerated chronic treatment with TAK-070, and the mean survival rates were at similar levels after ~6 months treatment by vehicle or TAK-070 (81% or 94%, respectively), without any differences in body weights and food consumption between cohorts.

We first quantitated the levels of Tris-soluble Aβ in the brains of untreated 13-month-old Tg2576 mice, which were dramatically increased by 68% and 129%, respectively for $A\beta_{40}$ and $A\beta_{42}$, compared with those at 8 months (Fig. 6*B*). Notably, the level of sAPPα was decreased by 32% at 13 months. Consistent with the results in young Tg2576 mice (Fig. 6*A*), TAK-070 reduced the levels of Tris-soluble $A\beta_{40}$ and $A\beta_{42}$ by ~15 and ~25%, respectively, and increased that of sAPPα by ~22% even after the 6 months of treatment (Fig. 6*B*).

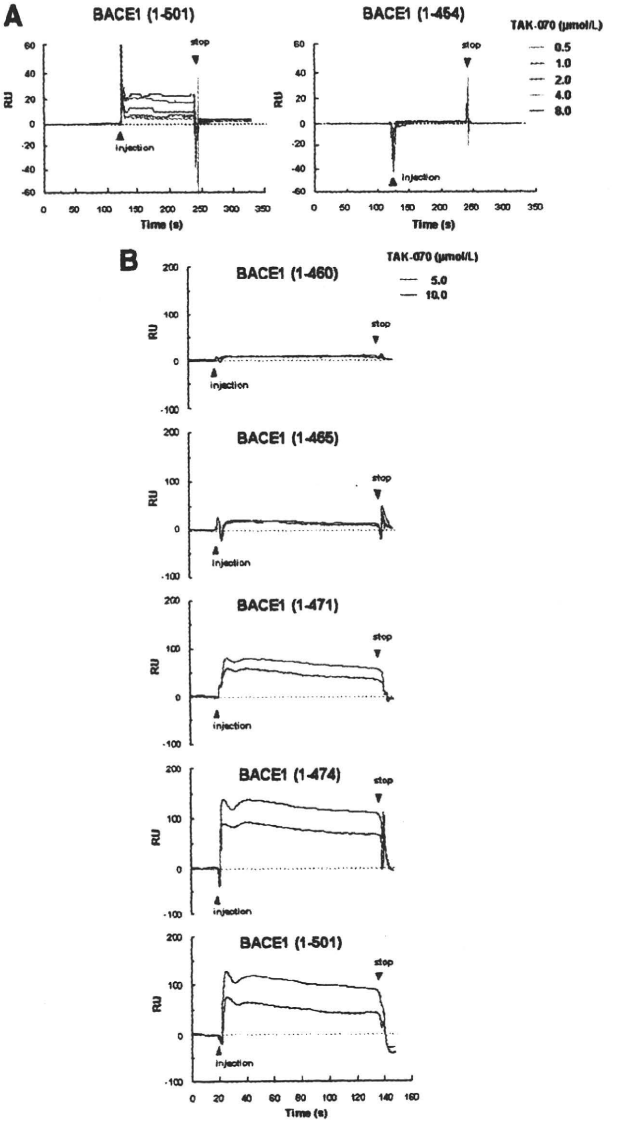

Figure 5. Surface plasmon resonance assay of the binding of TAK-070 to BACE1. ***A***, Sensorgram showing a binding of TAK-070 to full-length BACE1 (1-501) (left panel), but not to C-terminally truncated BACE1 (1-454) lacking the membrane spanning region (right panel). TAK-070 bound to full-length BACE1 in a concentration-dependent manner (within the range of 0.5–8 μmol/L). ***B***, Binding of TAK-070 (5 and 10 μmol/L) to full-length BACE1 (1-501) or C-terminally truncated BACE1 (1-474), (1-471), (1-465), and (1-460). One relative unit (RU) corresponds to 1 pg/mm^2.

We next quantitated the levels of insoluble Aβ that was extracted from the Tris-insoluble pellets by formic acid denaturation. The levels of insoluble $A\beta_{40}$ and $A\beta_{42}$ in untreated Tg2576 mice were markedly increased at 13 months by ~35-fold and ~23-fold, respectively, compared with those of young control mice (6367 ± 720 and 3513 ± 317 pmol/g wet weight, in 8 months of Tg2576). No gender differences were noted in the extent of age-related Aβ increase in our cohort (data not shown). Chronic TAK-070 treatment significantly reduced the levels of insoluble $A\beta_{40}$ and $A\beta_{42}$ by ~30% (Fig. 6*C*).

We then analyzed the effects of TAK-070 on the formation of Aβ plaques using immunohistochemistry and unbiased morphometric analysis. The numbers of Aβ plaques in the cerebral neocortex and hippocampus in TAK-070-treated cohort were markedly reduced